

“Lomonosov” Satellite—Space Observatory to Study Extreme Phenomena in Space

V.A. Sadovnichii¹ · M.I. Panasyuk² · A.M. Amelyushkin³ · V.V. Bogomolov² ·
V.V. Benghin³ · G.K. Garipov³ · V.V. Kalegaev³ · P.A. Klimov² · B.A. Khrenov³ ·
V.L. Petrov³ · S.A. Sharakin³ · A.V. Shirokov³ · S.I. Svertilov² · M.Y. Zотов³ ·
I.V. Yashin³ · E.S. Gorbovskoy⁴ · V.M. Lipunov⁵ · I.H. Park⁶ · J. Lee⁶ · S. Jeong⁶ ·
M.B. Kim⁶ · H.M. Jeong⁶ · Y.Y. Shprits^{7,8,9} · V. Angelopoulos¹⁰ · C.T. Russell¹⁰ ·
A. Runov¹⁰ · D. Turner¹⁰ · R.J. Strangeway¹⁰ · R. Caron¹⁰ · S. Biktemerova¹¹ ·
A. Grinyuk¹¹ · M. Lavrova¹¹ · L. Tkachev¹¹ · A. Tkachenko^{11,12} · O. Martinez¹³ ·
H. Salazar¹³ · E. Ponce¹³

Received: 11 May 2017 / Accepted: 19 September 2017 / Published online: 25 October 2017
© The Author(s) 2017. This article is published with open access at Springerlink.com

Abstract The “Lomonosov” space project is lead by Lomonosov Moscow State University in collaboration with the following key partners: Joint Institute for Nuclear Research, Russia, University of California, Los Angeles (USA), University of Pueblo (Mexico), Sungkyunkwan University (Republic of Korea) and with Russian space industry organi-

The Lomonosov Mission

Edited by Yuri Shprits, Hans Bloemen and Jim Burch

The original version of this article was revised due to a retrospective Open Access order.

- ✉ M.I. Panasyuk
panasyuk@sinp.msu.ru
- ✉ I.H. Park
ilpark@skku.edu

¹ Lomonosov Moscow State University, Moscow, Russia

² Physics Department, Skobeltsyn Institute of Nuclear Physics, Lomonosov Moscow State University, Moscow, Russia

³ Skobeltsyn Institute of Nuclear Physics, Lomonosov Moscow State University, Moscow, Russia

⁴ Sternberg Astronomical Institute, Lomonosov Moscow State University, Moscow, Russia

⁵ Physics Department, Sternberg Astronomical Institute, Lomonosov Moscow State University, Moscow, Russia

⁶ Department of Physics, Sungkyunkwan University, Seobu-ro, Jangangu, Suwon, Korea

⁷ Helmholtz Centre Potsdam, GFZ German Research Centre for Geosciences, Telegrafenberg, Potsdam 14473, Germany

⁸ Institute for Physics and Astronomy, University of Potsdam, Potsdam, Germany

⁹ Department of Earth, Planetary and Space Sciences, UCLA, 405 Hilgard Ave, Los Angeles, CA 90095, USA

¹⁰ Institute of Geophysics and Planetary Physics, UCLA, Los Angeles, CA, USA

zations to study some of extreme phenomena in space related to astrophysics, astroparticle physics, space physics, and space biology. The primary goals of this experiment are to study:

- Ultra-high energy cosmic rays (UHECR) in the energy range of the Greizen-Zatsepin-Kuzmin (GZK) cutoff;
- Ultraviolet (UV) transient luminous events in the upper atmosphere;
- Multi-wavelength study of gamma-ray bursts in visible, UV, gamma, and X-rays;
- Energetic trapped and precipitated radiation (electrons and protons) at low-Earth orbit (LEO) in connection with global geomagnetic disturbances;
- Multicomponent radiation doses along the orbit of spacecraft under different geomagnetic conditions and testing of space segments of optical observations of space-debris and other space objects;
- Instrumental vestibular-sensor conflict of zero-gravity phenomena during space flight.

This paper is directed towards the general description of both scientific goals of the project and scientific equipment on board the satellite. The following papers of this issue are devoted to detailed descriptions of scientific instruments.

Keywords Gamma-ray bursts · Ultra-high energy cosmic rays · Radiation belts · Space mission

1 Introduction

The “Lomonosov” space project was initiated and led by Lomonosov Moscow State University, a multi-disciplinary educational and leading scientific organization in Russia which directed the scientific goals of the space laboratory towards studying the most pertinent current space sciences issues, which are currently under development in MSU.

The following scientific topics will be studied with the Lomonosov mission:

- studying Ultra High Energy Cosmic rays (UHECR) with energies from 5×10^{19} to 10^{20} eV near the Greizen-Zatsepin-Kuzmin (GZK) energy cut-off;
- detecting Gamma-Ray Bursts (GRBs) between ultraviolet and gamma ranges to study optical prompt emission and precursors;
- studying transient UV phenomena in the upper atmosphere, as a continuation of research carried out by the previous MSU space projects: “Universitetsky-Tatiana,” “Universitetsky-Tatiana-2,” and Vernov; and
- studying the dynamics of magnetospheric particles, their acceleration, transport and loss processes and revealing their role in the generation of transient and quasi-stationary phenomena in the upper atmosphere within the X-ray and optical ranges.

Studies of extremely high energy and power processes such as ultra-high energy cosmic rays and gamma-ray bursts are of great importance not only for the understanding these phenomena, but also for the development of the theory of the early Universe.

Ultra-high energy cosmic rays (UHECR hereafter) are most likely produced by the Active Galactic Nuclei (AGN). The fundamental issue is estimating maximal particle energy, to which they could be accelerated in such sources, and whether there is a maximum energy to which particles can be accelerated in the Universe. Since AGN are very distant objects,

¹¹ Joint Institute for Nuclear Research, Dubna, Moscow Region, Russia

¹² Bogolyubov Institute for Theoretical Physics, Kiev, Ukraine

¹³ University of Puebla, Puebla, Puebla, Mexico

UHECR travel long distances before coming to the Earth. During their propagation, UHECR lose energy due to photo-production of secondary particles (mostly pions) on the microwave background photons. This leads to a natural limit of observable cosmic ray particle energy and to the UHECR energy spectrum cut-off at the photo-production energy threshold, i.e. about 5×10^{19} – 10^{20} eV (GZK (Greisen-Zatsepin-Kuzmin) cut-off). However, currently we have only limited and contradictory information on the energy spectrum and composition of the cosmic particles at energies at and beyond the GZK cut-off (cosmic rays around the GZK energy limit are called UHECR). Thus, it is not possible to make any final conclusions about the nature of UHECR, their source location or mechanism of acceleration.

Another extreme phenomena in the Universe are gamma-ray bursts (GRBs hereafter), which are observed as short (from dozens of milliseconds up to dozens of seconds) increases of gamma-fluxes. Discovered in the 1960s, they are still at the cutting edge of astrophysics. GRBs, which are the most powerful phenomena observed in the Universe, occur not only in gamma-range, but also in optics and UV. The power from the explosion of these most bright astrophysical objects achieves 10^{51} – 10^{53} erg/s. GRB optical emissions last up to several hours or even days, which can be evidence of afterglow, which appear after a giant explosion in the external shock wave expanding in the interstellar space and stellar wind of the exploded star. It is likely the collapse of a massive, fast-rotating star into a black hole in the case of so-called long-duration (more than a few seconds) bursts or the merging of neutron stars in a tight binary system in the case of so-called short-duration (less than a second) bursts. However, these models are under discussion, and the nature of this extraordinary phenomenon is still unknown. Due to the unusually powerful brightness of GRBs, studying their properties allows the researchers to explore the epoch of the early Universe, i.e. to study the evolution of the stars and the stellar populations within the wide range of red shift (cosmological distances) from $z \sim 0.1$ up to $z \sim 15$ – 20 .

Extreme phenomena occur not only in the far universe, but also in near-Earth space and even in the our planet’s atmosphere. Extreme phenomena include electron acceleration in the inner magnetosphere and precipitation, and the so-called Atmospheric Transient Energetic Phenomena (TEP), which are observed as Terrestrial Gamma-ray Flashes (TGF) and Transient Luminous Events (TLE) mostly in ultraviolet (UV). These phenomena are accompanied by short rising electron fluxes and electromagnetic emission bursts in wide frequency bands from radio to gamma-ray, including optical counterparts. TEP may be the consequence of physical processes resulting from different kinds of sudden energy release during short time intervals (from 10^{-6} to 10^{-3} seconds). Despite more than 20 years of experimental and theoretical research, there are no clear interpretations of such phenomena.

The dynamics of relativistic electrons in the Earth’s radiation belt can be considered a separate physical problem that includes electron acceleration, drift and loss processes caused by the radial diffusion, pitch-angle diffusion and energy diffusion. The study of relativistic electron dynamics also yields beneficial applications, as highly energetic relativistic electrons lead to internal charging that can result in and malfunction of electronic equipment or failure of satellite electronics.

The above mentioned issues with extreme phenomena studies dictate the scientific objectives of the considered space experiment and suggest a specific set of appropriate instruments.

Besides the above mentioned basic scientific goals of the Lomonosov project, we are planning to direct a portion of our experiments onboard the satellite to applied goals, including:

- studying multicomponent radiation doses along the orbit of spacecraft under different geomagnetic conditions;

- testing the space segment of the optical observation of the natural and artificial dangerous objects in near-Earth space;
- testing the automatic gaze stabilization corrector aimed at improving man's control of moving objects in microgravity conditions in space.

Scientific instruments with a total mass of 120 kg were installed onboard “Kanopus,” specially designed by JCK for the project, Research and production Corporation, Space Monitoring Systems, Information, & Control, and Electromechanical Complexes, named after A.G. Iosifian (VNIIEF Corporation, Russia). Kanopus was launched in on April, 28, 2016, from the new Russian space launching site Vostochny, by the Soyuz launch vehicle into Sun-synchronous orbit with an altitude of 550 km and an inclination of 98°.

This paper reviews the main scientific objectives of the project and the instrumentation onboard the Lomonosov spacecraft. More detailed information on the instruments will be presented in the following papers in this issue of the journal.

2 Ultra High Energy Cosmic Rays

2.1 Scientific Background

Since the registration of cosmic rays with energies of about 55 EeV (1 EeV = 10^{18} eV) at the MIT Volcano Ranch array (Linsley et al. 1961) and subsequent registration of additional energetic events with $E = 100$ EeV at the same experiment (Linsley 1963), many efforts have been placed on both experimental and theoretical studies of UHECR with $E \geq 50$ EeV. The nature and origin of these events still remain one of the greatest puzzles of modern astrophysics. The world's largest UHECR detector is the Pierre Auger Observatory (Auger for short), located in western Argentina. The observatory consists of 1,660 water Cherenkov detectors, which form the Surface Detector (SD) and 24 air fluorescence telescopes combined on four sites, which together constitute the Fluorescence Detector (FD). The water tanks are spread over 3,000 km² and separated by 1500 m on a hexagonal grid. Auger includes a denser infill array with 750 m between detectors, three high-elevation fluorescence telescopes and a few additional instruments (Aab et al. 2015c). The experiment began collecting data in 2004, and during ten years of operation its total exposure exceeded 50,000 km² sr yr (Valiño 2015). The observatory is operated by an international collaboration that includes institutions from 16 countries.

The second largest UHECR experiment is Telescope Array (TA), located in Millard County, Utah, USA. Similar to Auger, TA is using a hybrid technique of registering UHECRs, employing both fluorescence and surface detectors. In this case, the surface detectors are not water tanks, but 2-layer scintillators, each covering a 3 m² area. The surface array consists of 507 such detectors arranged on a 1.2 km square grid, covering approximately 680 km², i.e., $\sim 1/4$ of Auger. Three fluorescence detector stations are located in the corners of the surface array. They are instrumented with 38 telescopes (e.g., Fukushima 2015). After seven years in operation, the total exposure of TA equals 8,600 km² sr yr (Tinyakov et al. 2015). Telescope Array is an international collaboration of universities and research institutes of the United States, Japan, Korea, Russia, and Belgium. The experiment has been in operation since March 2008. It is planned to quadruple the area of the surface array up to approximately 3,000 km² by adding 500 more detectors with 2.08-km spacing (Sagawa 2015).

The most important feature of the UHECR flux is its energy spectrum. Soon after the first registration of extreme energy events, Greisen (1966) and, independently, Zatsepin and

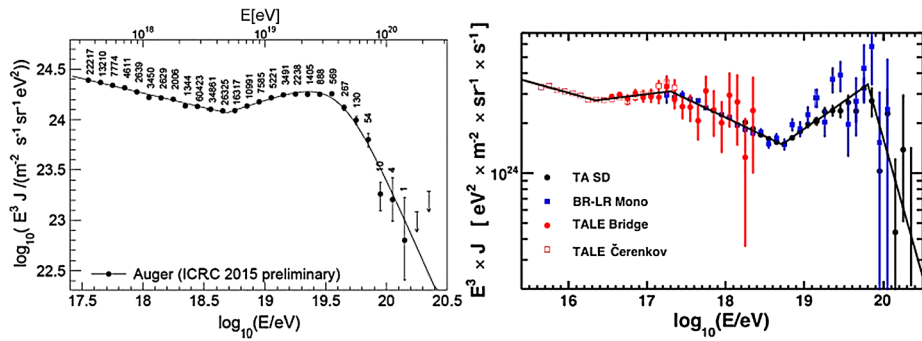


Fig. 1 *Left:* the combined energy spectrum of cosmic rays as measured by the Pierre Auger Observatory fitted with a flux model (Valiño 2015). The number of events is shown above the points, which are positioned at the mean value of $\lg(E/\text{eV})$. Only statistical uncertainties are shown. *Right:* energy spectrum measured by Telescope Array with four different techniques (Ivanov 2015), see the text for details

Kuz'min (1966) demonstrated that the flux of protons would be strongly suppressed at energies ≥ 50 EeV due to the photopion production on the cosmic microwave background radiation. For many years, the situation around the GZK cutoff was unclear and sometimes controversial until a predecessor of TA, the High Resolution Fly's Eye (HiRes) experiment, observed a suppression of the CR flux at ~ 60 EeV with a statistical significance of over 5σ (Bergman and High Resolution Fly's Eye Collaboration 2007; Abbasi et al. 2008). The remarkable discovery was soon confirmed by Auger (Abraham et al. 2008b) and later by TA (Abu-Zayyad et al. 2013b).

Since then, the energy spectrum of UHECRs has been measured with high statistics and accuracy. The latest combined energy spectrum as measured by Auger is shown in the left panel of Fig. 1 (Valiño 2015). The dominant systematic uncertainty of the spectrum stems from the overall uncertainty in the energy scale and equals 14%. The latest energy spectrum by Telescope Array is presented in the right panel of Fig. 1 (Ivanov 2015). The following spectra are presented: the spectrum obtained with the surface detector (“TA SD”) during the period from May 11, 2008 to May 11, 2015; spectrum calculated using data from two fluorescence stations working in monocular mode during the period from January 1, 2008 to December 28, 2014 (“BR-LR Mono”); and two spectra obtained by the Telescope Array Low Energy extension (“TALE Bridge” and “TALE Čerenkov”). It is seen that the spectra obtained by Auger and TA are similar above $\lg(E/\text{eV}) = 17.5$. Both experiments observe the so-called “ankle” at about 5 EeV and the suppression of flux at energies predicted by Greisen, Zatsepin and Kuz'min (GZK). A joint working group of the Pierre Auger, Telescope Array and Yakutsk collaboration concluded that the energy spectra determined by Auger and TA are consistent in normalization and shape within systematic uncertainties after energy scaling factors are applied (Dawson et al. 2013). There is a noticeable difference between the spectra related to the cutoff though; the steepening of the UHECR flux begins above approximately 30 EeV in the case of Auger, 60 EeV for TA, and the Auger spectrum is steeper than the TA spectrum above the GZK cutoff. The discrepancy in the energy spectra obtained by Auger and TA does not allow one to make final conclusion if the observed cut-off is due to the GZK effect or due to the maximum energy attained in accelerators of EECRs, or a combination of both (see Harari 2014 for an in-depth discussion).

Another important observable of UHECRs, crucial for identification of their sources, is the nuclear composition. It is mainly derived based on observations of the depth of maximum X_{max} (measured in g/cm^2) of extensive air showers (EAS) born in the atmosphere by primary

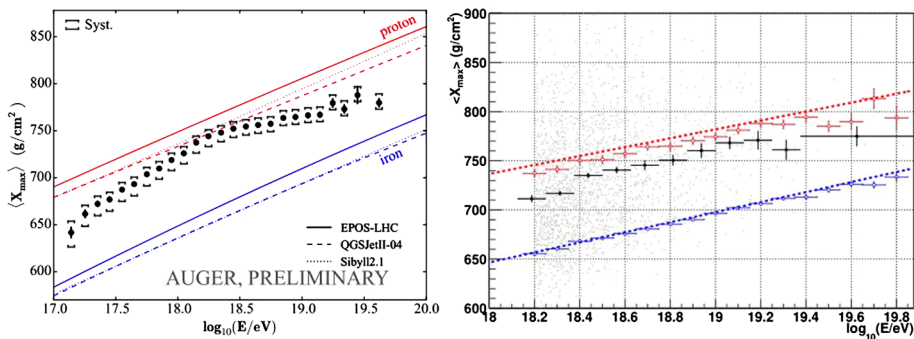


Fig. 2 Energy evolution of the mean of X_{\max} compared to MC simulations for proton (red) and iron (blue) primaries. *Left*: Pierre Auger Observatory (Porcelli 2015); *right*: Telescope Array (Hanlon and Ikeda 2015)

CR particles and Monte-Carlo (MC) simulations of EAS for different nuclear primaries. The mean value of X_{\max} is expected to scale with energy E and the mass number A of the primary particles as

$$\langle X_{\max} \rangle = a(\ln E - \ln A) + b.$$

The Pierre Auger collaboration has performed an intensive analysis of the distribution of X_{\max} using data collected in 2004–2012 with the FD (Aab et al. 2014a, 2014b). The energy dependence of the mean and standard deviation of the X_{\max} distributions were compared to MC simulations using a variety of hadronic interaction models. It was concluded that the flux of UHECRs is composed of mostly light nuclei at around 2 EeV and that the fraction of heavy nuclei is increasing up to 40 EeV (Aab et al. 2014a), but none of the existing hadronic interaction models can describe the data as a simple mixture of protons and iron nuclei (Aab et al. 2014b).

The Telescope Array collaboration also performs intensive studies of the chemical composition of UHECRs using information about X_{\max} . The reconstruction techniques employ observations obtained either by two of the fluorescence detectors (stereo mode) or by the surface array and one of the FDs (so-called hybrid mode). The latest hybrid composition measurements were based on the five-year data collected with the surface array and the Middle Drum site, which consists of 14 refurbished fluorescence telescopes of the earlier HiRes experiment. The analysis performed was similar in some methodology respects to Auger to simplify comparison between the results of the two experiments. Good agreement was found between data and a light, nearly protonic, composition, confirming the earlier HiRes stereo measurements. The elongation rate and mean values of X_{\max} found by TA were in good agreement with Auger data, but the TA data is incompatible with a pure iron composition over the whole available range of energies (Abbasi et al. 2015a). The latest results from both collaborations are presented in Fig. 2.

The seeming discrepancy between the results of Auger and TA on the nuclear composition of UHECRs attracted much attention, and a special working group of the collaborations was created. It should be noted that the measurement of masses of primary particles is one of the most difficult tasks in the physics of UHECRs, since it is based on hadronic interaction models at energies far beyond the reach of man-made accelerators like the LHC. On the other hand, Auger and TA employ different analysis techniques and different cuts selecting data for the analysis, so that a direct comparison of the results of the experiments

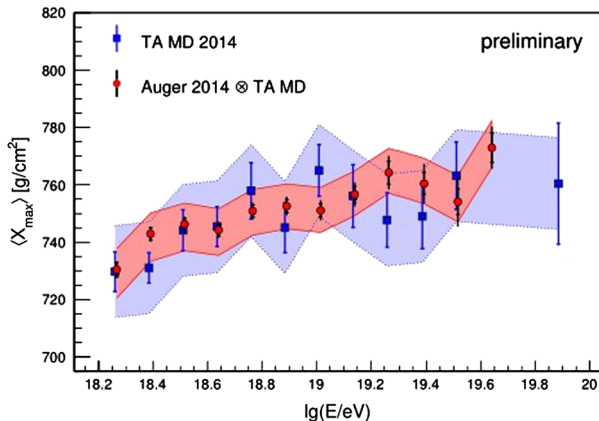


Fig. 3 Energy evolution of the mean of X_{\max} as measured with the Middle Drum site of TA (blue squares) and the Auger data folded with the MD acceptance (red circles). The data points are slightly shifted horizontally for better visibility. In the case of the Auger points, the inner error bars denote the statistical uncertainty of the measurement, and the total error bar also includes contributions from the limited statistics of simulated events used for the folding. The colored bands show the systematic uncertainties of the X_{\max} scales of each experiment (Abbasi et al. 2015b)

can be misleading. Namely, the TA collaboration published values of X_{\max} obtained from distributions of X_{\max} that included detector effects such as selection efficiency and acceptance. Interpretation of the data is made possible by the comparison of the MC predictions for proton and iron nuclei also folded with detector resolution and efficiency. In the analysis performed by Auger, only shower geometries are selected, allowing sampling of almost unbiased X_{\max} distributions. Residual biases from the acceptance, reconstruction and resolution are corrected for Abbasi et al. (2015b), Unger (2015). A thorough comparison of the energy evolution of X_{\max} as measured by TA and Auger has been performed by the working group. After accounting for the different resolutions, acceptances and analysis strategies of the experiments, the results were found to be in good agreement within systematic uncertainties (Fig. 3), but a more detailed analysis is in progress. Evidently, an experiment that could measure the energy spectrum and provide definite conclusions concerning the nuclear composition of UHECR primaries with high statistics and accuracy would be beneficial in cross-checking the results of Auger and TA.

One more aspect of cosmic rays physics that attracts much attention is anisotropy of arrival directions of EECRs. It is one of the key elements in the search for their possible sources but also an indirect probe of nuclear composition since light primaries of extreme energies are expected to be deflected very little by extragalactic magnetic fields on their path from sources.

One of the classical directions of anisotropy studies is the search for large-scale anisotropy of UHECRs. The Pierre Auger collaboration presented results of two Rayleigh analyses, one in the right ascension and one in the azimuth angle distributions, of the arrival directions of events with energy above 4 EeV and zenith angle up to 80° (Aab et al. 2015a) (see Fig. 4). The largest departure from isotropy was found in the $E > 8$ EeV energy bin, with an amplitude for the first harmonic in right ascension $(4.4 \pm 1.0) \times 10^{-2}$, which has a chance probability of 6.4×10^{-5} . It was found that assuming the only significant contribution to large-scale anisotropy is from the dipolar component; the observations above 8 EeV correspond to a dipole of amplitude 0.073 ± 0.015 pointing to $(\alpha, \delta) = (95^\circ \pm 13^\circ, -39^\circ \pm 13^\circ)$,

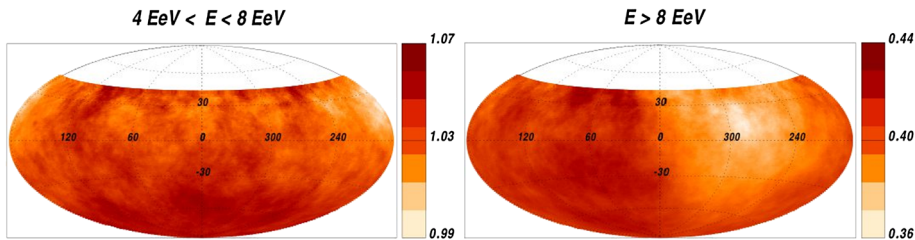


Fig. 4 Auger sky map of UHECR flux, in $\text{km}^{-2} \text{yr}^{-1} \text{sr}^{-1}$, smoothed in angular windows of 45° radius, for events with energies $4 < E < 8 \text{ EeV}$ (left) and $E > 8 \text{ EeV}$ (right). Equatorial coordinates are used (Aab et al. 2015a)

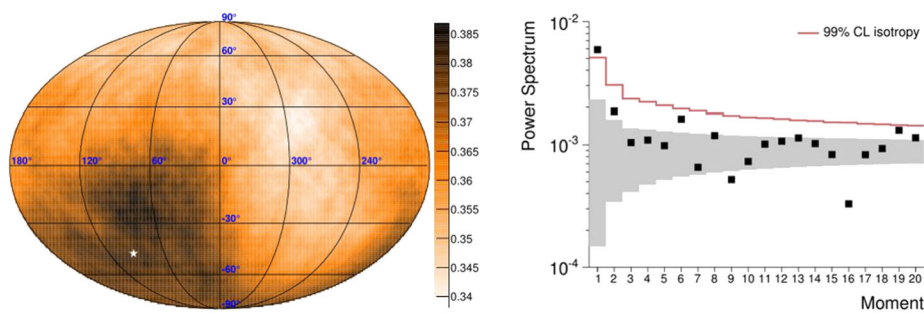


Fig. 5 Left: joint Auger-TA sky map in equatorial coordinates, in $\text{km}^{-2} \text{yr}^{-1} \text{sr}^{-1}$, of the average flux smoothed in angular windows of 60° radius, for events with energies above 10 EeV. The white star shows the direction of the reconstructed dipole. Right: joint Auger-TA angular power spectrum (Deligny 2015)

thus supporting an earlier result obtained for events with zenith angles $< 60^\circ$ (de Almeida 2013). The result was updated recently but the conclusions remained unchanged (Al Samarai 2015).

Telescope Array has also performed an analysis of large-scale anisotropy of cosmic rays at the highest end of the spectrum, though a totally different approach was employed by Fukushima et al. (2013). Assuming pure proton composition, it was found that the distribution of events with energies $> 10 \text{ EeV}$ and $> 40 \text{ EeV}$ is compatible with the hypothesis of isotropy and incompatible with the distribution of the local large-scale structure (LSS) at smearing angles smaller than $\sim 20^\circ$ and $\sim 10^\circ$ respectively. On the contrary, the data set composed of events with energies above 57 EeV was found to be compatible with the LSS model and incompatible with isotropy at the (pre-trial) statistical significance $\sim 3\sigma$.

Studies of large-scale anisotropy can present complications because none of the experiments observe the whole celestial sphere; a proper determination of the full set of multipole coefficients requires full-sky coverage. This is why a joint analysis of large-scale anisotropy of UHECRs with energies above 10 EeV performed by the TA and Pierre Auger collaborations is of specific interest (Aab et al. 2014c; Deligny 2015). A declination band commonly covered by both experiments was used for cross-calibrating the fluxes. No significant deviations from isotropy expectations were found at any angular scale, but upper limits on the amplitudes of the dipole and quadrupole moments were reported as a function of the direction in the sky. The latest result is shown in Fig. 5. The analysis employed 2,560 events with zenith angles $< 55^\circ$ and energies above 10 EeV registered during 6 years of operation by TA and 16,835 events with zenith angles $< 80^\circ$ and energies above 8.8 EeV collected during

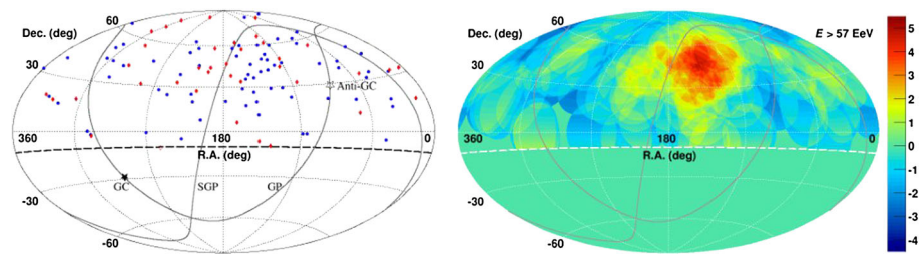


Fig. 6 *Left:* arrival directions of UHECRs with energies above 57 EeV as registered by Telescope Array, in equatorial coordinates. *Blue points* indicate the 5-year data, and *red diamonds* indicate events observed during the 6th and 7th years of data collection. *Right:* significance map for the 7-year data smoothed in angular windows of 20° radius (Kawata et al. 2015)

10 years of operation by Auger. The dipole amplitude was found to be $(6.5 \pm 1.9)\%$ with a chance probability 5×10^{-3} , pointing to $(93^\circ \pm 24^\circ)$ in right ascension and $(-46^\circ \pm 18^\circ)$ in declination. Interestingly, the angular power spectrum obtained in the latest study by Deligny (2015) demonstrated the dipole moment standing out of the background noise, in contrast with the earlier study by Aab et al. (2014c), which did not reveal any significant deviation from isotropy. The quadrupole amplitudes were observed to be within statistical fluctuations expected from isotropic samples.

Anisotropy studies are also performed at smaller angular scales in search of correlation with the LSS in the local universe and possible sources of UHECRs. Much attention was attracted to a correlation between the arrival directions of cosmic rays with energies above 55 EeV and the distribution of active galactic nuclei (AGN) within 75 Mpc, among them the Centaurus A (Cen A) radiogalaxy, located at less than 4 Mpc distance, reported by the Pierre Auger Collaboration (Abraham et al. 2007, 2008a; Abreu et al. 2010). More recently, Auger presented results of a whole number of tests aimed to the search for signals of anisotropy of cosmic rays with energies above 40 EeV (with 231 of them having energies ≥ 52 EeV and zenith angles $< 80^\circ$) (Aab et al. 2015b). None of the tests performed revealed a statistically significant deviation from isotropy, but it was found that there is a certain excess of events with energies ≥ 58 EeV around the direction to Cen A and around AGN of the Swift catalogue within 130 Mpc and brighter than 10^{44} erg s $^{-1}$. In both cases, the probability of the excess arising by chance was estimated to be of the order of 1.3–1.4%. On the other hand, a similar study performed by TA using UHECRs with energies ≥ 40 EeV registered by the surface detector during the first 40 months of its operation did not reveal any statistically significant correlations with AGN from a number of survey catalogues (Abu-Zayyad et al. 2013a).

The most intriguing new result in anisotropy studies is the discovery of a “hotspot” of CRs with energies above 57 EeV made by TA (Abbasi et al. 2014). The hotspot reported was a cluster of 19 (of 72 events registered during 5 years of observations) events within a 20° radius circle centered at (equatorial coordinates) $(\alpha, \delta) = (146.^\circ 7, 43.^\circ 2)$ with an expected number of events equal to 4.49, which gives a (pre-trial) statistical significance of 5.1σ . The (post-trial) statistical significance of such a hotspot appearing by chance was estimated to be 3.4σ . Two more years of observations confirmed the existence of the hotspot, but did not increase the statistical significance of the departure from the expected isotropic background; with 24 events making the hotspot, the estimated number of background events equals 6.88 (Kawata et al. 2015), and this gives the same significance as before. Figure 6 illustrates the latest result.

The hotspot is located near the Supergalactic plane, but there are no known specific sources behind it. It was suggested by the TA Collaboration that the hotspot may be associated with the closest galaxy groups and/or the galaxy filament connecting the Milky Way with the Virgo cluster; or, if UHECRs are heavy nuclei in accordance with the Auger results, the hotspot events may originate in the Supergalactic plane and be deflected by the magnetic fields (Abbasi et al. 2014).

Detection of the TA hotspot with higher statistical significance than currently obtained (3.4σ) requires an increased number of collected events. Unfortunately, the Pierre Auger Observatory cannot aid in this task since the hotspot is only partially covered by its field of view and only with the most inclined events. One of the opportunities to increase statistics is promised by the planned extension of the surface detector of Telescope Array. A viable opportunity to arrange an independent test of the result concerning the TA hotspot is employing an orbital experiment. Thus the question is whether KLYPVE or JEM-EUSO will be able to solve the task.

The question was recently considered by Semikoz et al. (2016), who performed MC simulations based on the TA 5-year data and estimations of exposure of the JEM-EUSO telescope by Adams et al. (2013), which are applicable to the KLYPVE detector since both are planned to be installed on the International Space Station and share the same principles of observing extensive air showers from space. It was demonstrated that if the detected luminosity of the hotspot is attributed to a physical effect and not a statistical fluctuation, the KLYPVE and JEM-EUSO experiments would need to collect approximately 300 events with energies above 57 EeV over the whole celestial sphere in order to detect the hotspot at the 5σ confidence level with 68% probability. It was estimated by Olinto et al. (2015) that with the annual exposure $\sim 5 \times 10^4 \text{ km}^2 \text{ sr}$ above $\sim 60 \text{ EeV}$, JEM-EUSO will collect 429 events/yr, or about 2,145 events in 5 years. KLYPVE will have the annual exposure $\sim 1.2 \times 10^4 \text{ km}^2 \text{ sr}$ above 50 EeV (Panasyuk et al. 2015; Sakaki et al. 2015) and thus will be able to detect more than 100 events every year of operation, and more than 600 events during its planned lifetime. It was concluded that with its huge annual exposure (almost an order of magnitude larger than that of the Pierre Auger Observatory) and the planned 5-year operation time, JEM-EUSO has excellent opportunities for confirming the existence of the TA hotspot at high confidence level. In 6 years of operation, KLYPVE will have obtained the total exposure, approximately 1/3 of JEM-EUSO, and thus it also has a strong discovery potential, especially if the 5-year flux registered by the Telescope Array persists.

As shown above, a considerable part of the difficulty in obtaining definite conclusions concerning anisotropy of UHECRs and finding their sources is due to the limited statistics of events and the incomplete and non-uniform coverage of the celestial sphere by any of the modern experiments. Therefore, one must increase the statistics of UHECRs providing a uniform exposition of the sky. This is exactly the field where orbital experiments are able to open new, very promising horizons of research, not to mention a number of other scientific tasks related to astrophysics, fundamental physics and atmospheric sciences.

2.2 Method of Measurements

In our experiment, the Earth's atmosphere will be used as a "detector" of UHECRs, which produce cascades of secondary particles, i.e. extensive air (or Auger) showers (EAS), which can provide us information about the primary particle parameters. The bulk of secondary particles in EAS ionize and excite molecules of atmospheric nitrogen and oxygen and lead to the so-called ionization glow, which is most intensive along the EAS axis and resembles a track breaking out in a very short time (about several microseconds). The fluorescence

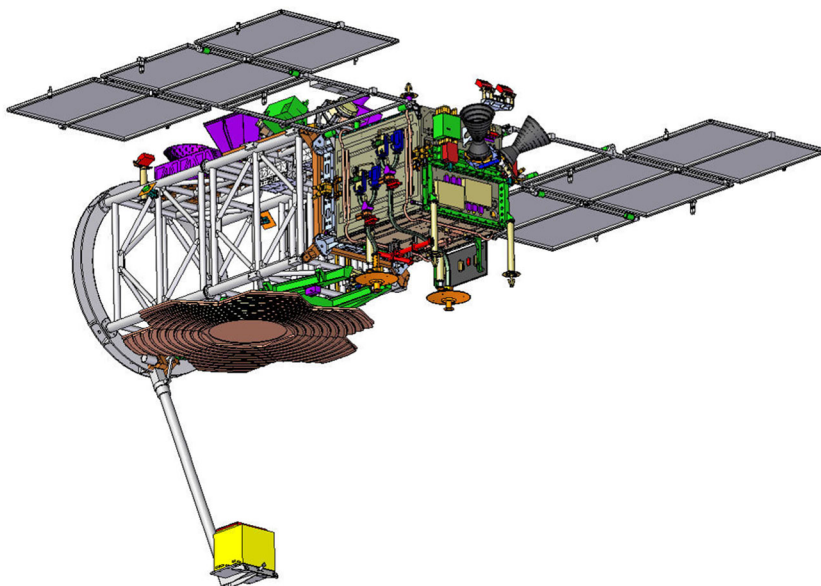


Fig. 7 The UHECR detector TUS on bottom of the Lomonosov satellite platform. The TUS telescope has the segmented mirrors with 256 pixels photo receiver at the focal plane

intensity and its timing along the UV track provide information on EAS cascade development, direction and energy of primary particles. All of these tasks were fulfilled by imaging fluorescence detectors developed for ground-based EAS arrays.

Existing ground-based experimental arrays do not collect statistically confident data on UHECR—especially beyond the GZK energy limit. New methods of UHECR observation with two orders of magnitudes larger exposure are needed to solve this problem. The method of EAS fluorescence observation from satellites proposed by Linsley and Benson (1981) may become such a technique. For testing the new method of the UHECR study, the Russian team (SINP MSU, JINR-Dubna and Space Regatta Consortium) and universities in Korea and Mexico have prepared space-based detector TUS (Tracking Ultraviolet Setup) for launching on board the Lomonosov satellite for testing the new method (Fig. 7).

Space-based detectors have the following advantages:

- (1) UHECR particle track can be observed on a large area of the atmosphere from a great distance to the atmosphere. At orbit altitude of the Lomonosov satellite (500 km), the TUS detector, will survey an approximately $6,400 \text{ km}^2$ area of the atmosphere.
- (2) In one (or more) year of its in-orbit operation, the same detector observes the entire celestial sphere. This will allow for the study of the distribution of UHECR sources, despite possible inaccuracy of determining primary particle energy. An unavoidable difference in absolute value of the energy measured by different ground-based arrays causes a difference in UHECR intensity in different sky regions covered by different arrays.

At the same time, the detector onboard the satellite encounters a number of difficulties:

- (a) Observation of EAS from a distance approximately 10 times greater than in ground based experiments requires higher sensitivity and resolution of optical system and of photo detector. Desirable resolution of one detector pixel should be equal to diameter of

lateral electron distribution in a shower. For a satellite orbit height of 500 km, the angular resolution of the orbital detector should be 0.4–2 mrad, which is an order of magnitude higher than that of the existing ground-based detectors (20 mrad).

- (b) Nighttime atmosphere noise in UV band (300–400 nm) used for EAS detection varies on satellite route. The data from Universitetsky-Tatiana satellite (Sadovnichy et al. 2011) gave scale of such variation: from 3×10^7 – 2×10^8 photon $\text{cm}^{-2} \text{sr}^{-1} \text{s}^{-1}$ —at moonless night (lower value—above oceans, higher value—above aurora zones and cities) to 2×10^9 photon $\text{cm}^{-2} \text{sr}^{-1} \text{s}^{-1}$ —at full moon night. Ground-based arrays are operated at moonless nights at specially chosen locations with noise level not more than 5×10^7 photon $\text{cm}^{-2} \text{sr}^{-1} \text{s}^{-1}$.
- (c) During flight at low latitudes, where electric activity of the atmosphere is high, impulsive noise from lightning and accompanying high altitude discharges will add to average noise level (see below).
- (d) Technology of an orbital fluorescence detector should satisfy complex conditions of space operation.

Bearing these difficulties in mind a program for gradual conversion of UV fluorescence detector in ground-based version to space version was started (Khrenov et al. 2001). TUS detector is the first, comparatively “simple”, instrument that will approve reliability and stability of optical system and photo detector design for operation in space.

3 Transient Atmospheric Events in UV as a Geophysical Phenomenon and as a Background in Fluorescence Method of Extreme Energy Cosmic Ray Measurements

TUS instrument will be also able to detect so-called “Transient Luminous Events” (TLEs) in the upper atmosphere. The nature of TLEs is probably associated with atmospheric electric-ity phenomena. During the high-altitude electric discharges between the clouds in the upper atmosphere and the clouds and ionosphere (altitudes from 5–10 km to 60–90 km) short-time (duration from one up to hundreds of milliseconds) bursts of electromagnetic radiation within wide spectral range (from visual light up to UV and even X-rays and gamma-rays) are observed. Current experimental data about the discharges in the upper atmosphere have shown that these phenomena are global, a number of discharges and the energy released in these discharges are so high that we can expect certain relations between the discharge phenomena and other geophysical phenomena.

Data on transient atmospheric ultraviolet radiation are of interest as in view of getting data on geophysical effects in the atmosphere so as a background in fluorescence method of extreme energy cosmic rays (EECR) measurement. In this method, fluorescence of nitrogen molecules in near ultraviolet range (wavelengths 320–420 nm) excited by EAS electrons is measured. Data on the atmosphere transient background are very im-
portant in case of detectors looking to the atmosphere downward from a satellite. EECR detector TUS (Tracking Ultraviolet Set-up) installed on the Lomonosov spacecraft will measure very low fluorescence photon numbers per EECR primary particle $Q \sim 10^{17}$ (to compare with number of photons $Q > 10^{23}$ usually measured as TLEs). TLE are of in-
dependent interest as geophysical phenomenon related to important geophysical problem of global electric current (via electrical discharges in the atmosphere). Aiming to fulfil both tasks: measurement of transient events as a background for planning fundamental physics experiment on the highest energy cosmic rays and study of geophysical problem



Fig. 8 Frame of web camera registering Elves type transient (upper event in this figure) and lightning below it (Kuo et al. 2007)

of global electric circuit, UV fluorescence detectors were put on boards of several MSU microsatellites. They are “Universitetsky-Tatiana” (Sadovnichy et al. 2007; Garipov et al. 2005, 2011), “Universitetsky-Tatiana-2” (Sadovnichy et al. 2011; Vedenkin et al. 2011; Garipov et al. 2013) and “Vernov” (Panasyuk et al. 2016). Their data will be widely used in this review. Titles of the first two satellites in the following text will be shortened to “Tatiana” and “Tatiana-2”. Expected data from Lomonosov detector TUS are briefly discussed here, for more detailed TUS description and expected performance see Klimov et al. (2017) in this issue.

3.1 Scientific Background. Phenomenology of Transient Atmospheric Events (TAE)

For observation from space, transient UV events generated in the upper atmosphere are in more favorable conditions, as they are less absorbed in route from event to detector. Electric discharges in the upper atmosphere—potential source of UV transients, a-priori, have higher chances to be detected by space detector. In the upper atmosphere lower ionosphere (D-layer) starts and its free electrons, accelerated by electromagnetic pulses coming from the atmosphere, are add to development of transients at these altitudes. Fluorescence of nitrogen molecules at UV levels, excited by electrons of low energies of 3–4 eV and much kind of events with comparably low electric field may produce detectable UV events in space detector. Lightning discharge is a source of gigantic EM impulse, which can produce bright transients detectable by a video camera with aperture of about 1 cm^2 and photo sensor with several megapixels. Events measured by video camera were historically the first (Franz et al. 1990) to discover subject of transient luminous events (TLE) as phenomenon of the atmosphere discharge between thunderstorm clouds and ionosphere initiated by lightning. Later on less luminous transient were discovered and we prefer here to call transients reviewed here as transient atmospheric events (TAE) meaning transient in wide scale of brightness. In this terms TLE are the brightest events among many less bright transient events.

Shooting TLE in direction perpendicular to its development it was discovered that in most cases an event in the upper atmosphere is accompanied by lightning below it. In Fig. 8 one frame of ISUAL camera operated on board Formosat-2 satellite (Kuo et al. 2007) shows both: transient of Elves type and scattered in the cloud lightning emission below it.

Elves type of transient was explained as a result of lightning electromagnetic pulse (EMP) crossing D-layer of the ionosphere (Kuo et al. 2007). Temporal profiles of signals in different wave length bands for Elves type event are presented in Fig. 9. Another type of TLE—Sprites—was also observed by video camera. One of the most informative pictures was obtained by high speed camera (frame period is 0.2 ms) by Cummer et al. (2006), see Fig. 10. As it is seen in Fig. 10 the Sprite starts to radiate as Elves—high in the atmosphere, in D-layer of ionosphere. Here EMP of lightning accelerates free electrons, existing

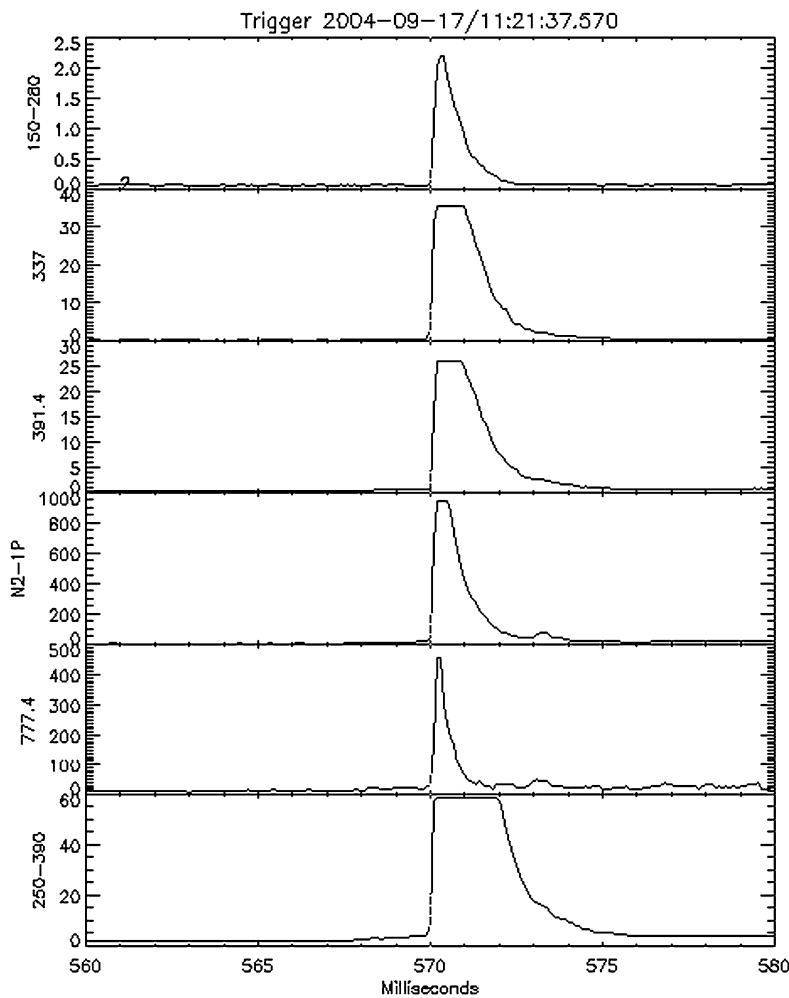


Fig. 9 Temporal profiles of signals in different wave length bands for Elve event presented in Fig. 8. Duration of Elves in all bands is ~ 1 ms (Kuo et al. 2007)

in the ionosphere. In this first stage, fluorescent glow develops upward—as EMP does. In the next stage electric field in the upper atmosphere—between thunderstorm clouds and ionosphere—plays significant role. This field is a result of lightning cloud-ground stroke canceling the electric field between ground and clouds changing it to a field between clouds and ionosphere. New field is longer in time (tens of milliseconds)—it exists until neighbor clouds electricity restore a general electric field in a thunderstorm. Between ionosphere and clouds slower transient starts to be developed downward (frame 4 and farther on in Fig. 10). In some extreme cases Sprite becomes a gigantic transient like in Fig. 11a, measured by Stenbaek-Nielsen et al. (2000). In their work not only very bright TLE was proved to exist but also ability of one lightning to generate several TLE was demonstrated. Other example of bright transient (called Gigantic Blue Jet) measured by Su et al. (2003) is presented in Fig. 11b.

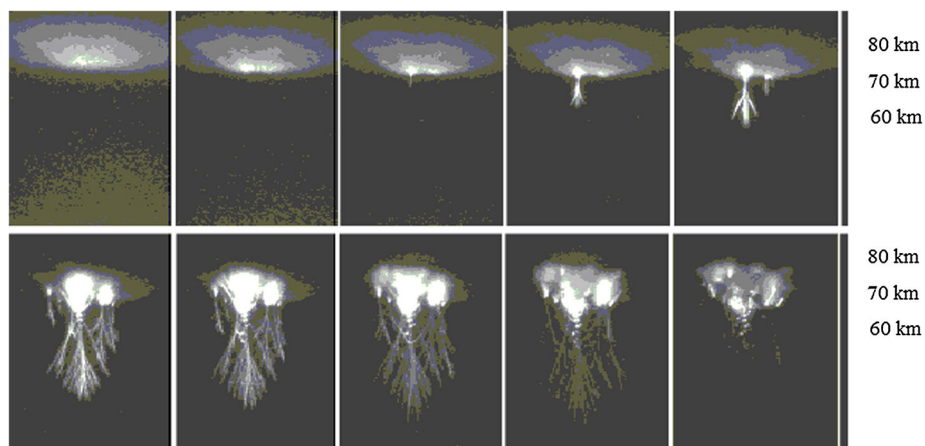


Fig. 10 Camera frames registering transient of Sprite type (Cummer et al. 2006). Camera frame—0.2 ms

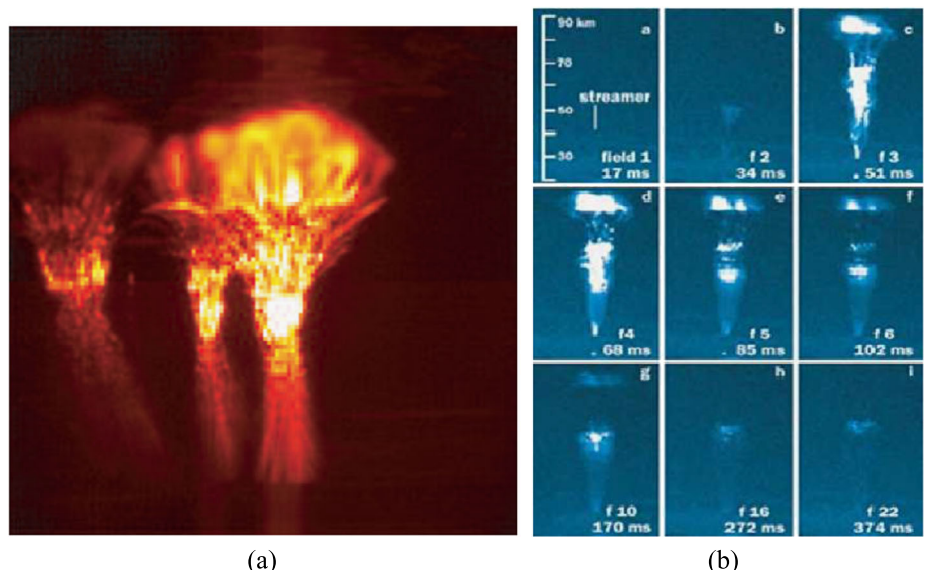


Fig. 11 Bright Sprites observed by Stenbaek-Nielsen et al. (2000) (a) and Gigantic Jet (b) from Su et al. (2003)

In another transient phenomenon—a Blue Jet—blue glow rises not so high—up to 40 km. There are indications that Blue Jets are not a direct consequence of neither positive nor negative lightning (Wescott et al. 1998). However, they occur over clouds in thunderstorm area and in time close to lightning (few seconds).

TLE observations by cameras gathered a basic knowledge about transient development which helps to interpret data obtained with simpler detectors like detector of UV radiation (DUV) on board of MSU micro satellites (Garipov et al. 2006). Data from DUV are temporal profiles of UV signal from transient obtained by photomultiplier with field of view of 15° in nadir direction. Examples of DUV transient temporal profiles measured on board

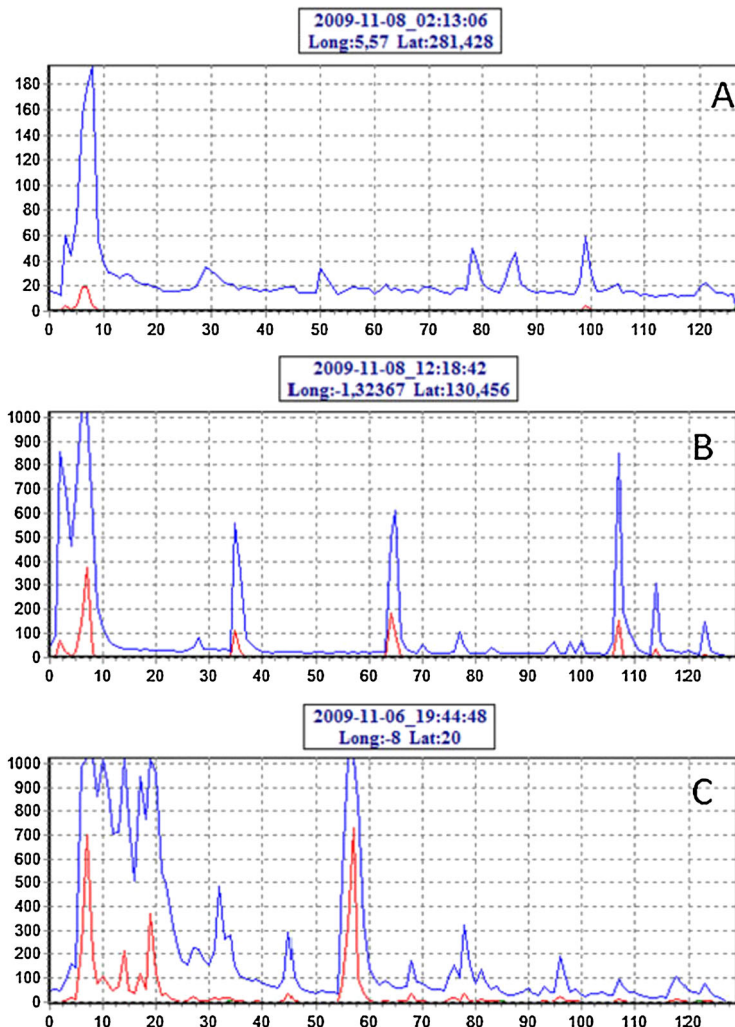


Fig. 12 Examples of transient temporal profiles. *Blue lines*—UV band. *Red line*—Red-Infra Red band. Y-axis—ADC code for measured transient integral photon number, X-axis—time in ms

Tatiana-2 satellite are shown in Fig. 12. Short (~ 1 ms) pulses in panels A and B could be interpreted as TAE of Elves type. Longer in time TAE (panel C) was interpreted as a Sprite. Distribution of all registered events in the Earth map, shown in Fig. 13, demonstrates strong correlation of TAE with lightning map—most of events are above continents in equatorial regions of the Earth. Data on ratio of TAE intensity in UV and Red-infrared bands (available in Tatiana-2 experiment Sadovnichiy et al. 2011; Vedenkin et al. 2011; Garipov et al. 2013) favor the transient origin of registered events—not lightning itself. This conclusion is based on temporal structure of events and their spectrum different from lightning spectrum (measured in Orville and Henderson 1984) and closer to sprite spectrum (Milikh et al. 1997). For more reliable conclusions study of lightning and other TAE spectra is needed—especially in UV range.

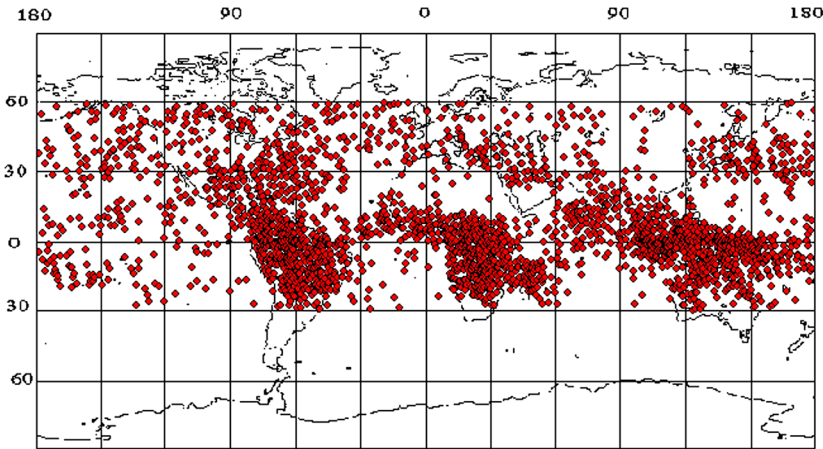
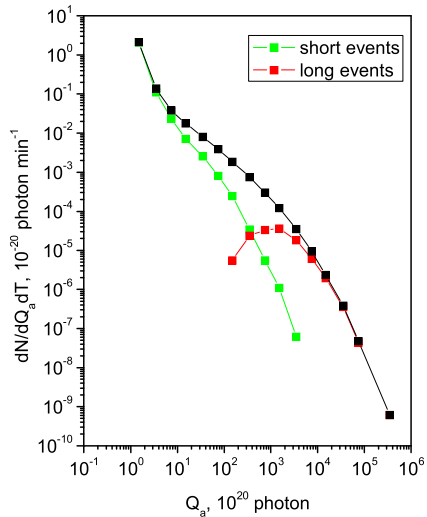


Fig. 13 TAE distribution in the Earth map (Garipov et al. 2013)

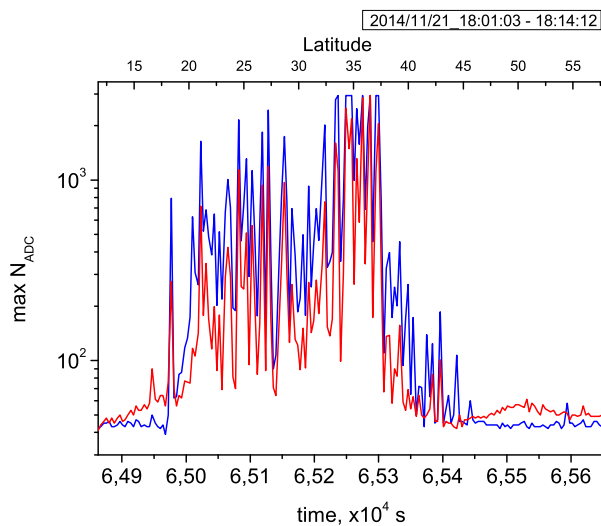
Fig. 14 Transient photon number distribution in the atmosphere. *Green*—short (less than 5 ms) events, *red*—long events



For triggering DUV by TAE, signal amplitudes in time bins (1 ms in Tatiana-2 experiment and 0.5 ms—in Vernov experiment) were compared and their maximum value in time period T ($T = 1$ min in Tatiana-2 experiment and $T = 4.5$ s in Vernov experiment) was a “triggering” criterion (in fact oscilloscope waveform of TAE was recorded every time T). In both experiments signal sum in oscilloscope trace of 128 ms was a measure of transient number of photons. The photon number radiated in the atmosphere Q_a was calculated from value of signal sum taking into account space detector distance to the atmosphere in assumption of isotropic radiation of TAE fluorescence.

In Fig. 14, transient distribution on the number of photons Q_a in the atmosphere is presented as it was measured in the Vernov experiment. Black squares represent all data; also represented is data for short TAE (duration less than 5 ms, green squares, and for longer TAE—red squares). One can see that short transients are numerous and have fewer UV

Fig. 15 Example of series of TAE in the Vernov experiment (blue curve—UV-emissions and red—infrared one)



photons than longer ones. It was also shown in Garipov et al. (2013) that short TAE are not concentrated to equatorial latitudes as longer ones. Whether this is a triggering effect or a physical phenomenon will be clarified during measurements onboard the Lomonosov satellite.

In the Vernov experiment, parameter T in the trigger condition is smaller than in the Tatiana-2 experiment, which makes the photon number “threshold” less. For $T = 60$ s in Tatiana-2, the experiment “threshold” Q_{ath} in photon number distribution was $Q_{ath} = 10^{21}$ (Garipov et al. 2013), while in the Vernov experiment ($T = 4.5$ s) Q_{ath} is shifted to 10^{20} . In the upcoming TUS experiment, the threshold photon number is expected to be $\sim 10^{17}$ —close to the fluorescence photon number in EAS of GZK (Greisen-Zatsepin-Kuzmin) energies.

The range of Q_a values measured in the MSU satellite experiments is very wide due to automatic control of photomultiplier gain applied over various intensities of the background atmosphere glow—from intensities of less than $10^8 \text{ cm}^{-2} \text{ s}^{-1} \text{ sr}^{-1}$ at moonless nights to $3 \times 10^9 \text{ cm}^{-2} \text{ s}^{-1} \text{ sr}^{-1}$ at full moon nights. The measured “hard” distribution over Q_a indicates an important TAE feature: the main energy released by TAE in the atmosphere is due to the brightest events of $Q_a > 10^{23}$ whose rate is close to the rate of TLE. In experiments Tatiana-2 and Vernov, TAE at large thunderstorm regions were regularly observed as a series of events registered every period T , the smallest technically required period between registered events. An example of such series detected by DUV onboard the Vernov satellite is shown in Fig. 15. Here, values of maximum signals in one bin of the oscilloscope trace, triggered every 4.5 s, are shown. Blue and red lines correspond to UV and Red-IR wave bands, respectively. The average rate of lightning available from LIS data (Christian et al. 1999) for the thunderstorm region is much lower than the observed transient rate in the series. Moreover, in some series, TAE are observed in clear atmosphere (no clouds), which is against lightning origin of those TAE. Analysis of correlation between clouds and any TAE (in series or not) is also in contradiction to the lightning origin of some TAE. An equal numbers of transients in both cloudy and cloudless areas of the atmosphere (Vedenkin et al. 2011; Garipov et al. 2013) were observed, while lightning was strongly correlated to clouds. Those data will be confirmed by new measurements with better identification of TAE and lightning.

3.2 Method of Measurements

The TUS detector onboard the Lomonosov satellite will provide new data on TAE due to large aperture of TUS and its ability to measure TAE images. Spatial resolution is 5 km at an atmospheric area of $80 \times 80 \text{ km}^2$. Temporal resolution varies from microseconds at the early stage of TAE to hundreds of milliseconds at its late stage (see article by Klimov et al. 2017, this issue).

4 Observation of GRBs

GRBs are the most luminous explosions in the Universe, emitting high-energy photons, and are detected at the highest redshift of any discrete source in the Universe (Salvaterra et al. 2009; Tanvir et al. 2009). These properties provide great leverage in time, wavelength, and information, and thus a unique opportunity to understand not only the nature of the Universe but fundamental physics (Lamb and Reichart 2000; Bromm and Loeb 2006; Kistler et al. 2009; Amati et al. 2008; Ghirlanda et al. 2006; Panaiteescu and Vestrand 2008; Kocevski 2012; Shahmoradi and Nemiroff 2011; Bernardini et al. 2012; Zhang et al. 2009; Greiner et al. 2011). Therefore the observation of GRBs in multi-wavelength is essential to the complete understanding of GRBs. The Lomonosov satellite is equipped with the instruments that are capable of the multi-wavelength observation of GRBs. The principle for the multi-wavelength observation of GRBs exercised in the Lomonosov satellite is to have a co-aligned system of an X-ray/gamma-ray detector and a UV/optical detector. The X-ray/gamma-ray detector detects X-rays or gamma-rays from GRBs to trigger and localize GRBs while its counterpart, the UV/optical detector, detects UV or optical photons from GRBs. There are two such co-aligned systems in the Lomonosov satellite. One co-aligned system is a gamma-ray monitor called the BDRG (Block for X-ray and gamma-radiation detection) plus two optical cameras called the SHOK (Optic cameras of super-wide field of vision) (Svertilov et al. 2017; Lipunov et al. 2017, this issue). The other co-aligned system is the Ultra-Fast Flash Observatory (UFFO) which consists of a coded mask X-ray telescope and a Ritchey-Chretien telescope with a fast slewing mirror for redirection of UV/optical photons onto it (Park et al. 2013). The coded mask X-ray telescope in the UFFO is called the UFFO Burst Alert Telescope (UBAT) while the Ritchey-Chretien telescope with a fast slewing mirror in the UFFO is called the Slewing Mirror Telescope (SMT) (Jeong et al. 2013). These two systems are described in Sect. 4.2.

4.1 Scientific Background

The emission of GRBs spans some 9 orders of magnitude in photon energy, a prime opportunity for synoptic observations. GRBs are believed to be sources of ultra-high energy cosmic rays (UHECR) (Waxman 2006; Abu-Zayyad et al. 2012; Tokuno et al. 2012; Abraham et al. 2004; Panasyuk et al. 2012; Takahashi 2009; Halzen and Klein 2010; Gorham et al. 2009) and gravitational waves (GW) whose detection has been reported recently (Cutler and Thorne 2002; Abramovici et al. 1992; Abbott et al. 2016a), and is a prime example of multi-messenger astronomy. The rapid-response in the observation of electromagnetic counterparts to GW (Abbott et al. 2016b) is important to obtain the rich information in physical processes of GRBs giving rise to each messenger and the time delay between them. In spite of the wide knowledge already acquired about GRBs from space (Fishman 1994; Boella et al. 1997; MacFadyen and Woosley 1999;

Ricker et al. 2002; Winkler et al. 2003; Gehrels et al. 2004; Perna et al. 2003; Piran 2004; Nakar 2007) and on ground there are still many open questions about their progenitors and environment. Deeper understanding of GRBs requires more statistics of GRBs, particularly of high-z GRBs, measurements of polarization, and a wider range of not only spectral coverage extending to sub-keV X-ray and infrared (IR) but also temporal coverage through rapid pointing of telescopes at GRBs. These observational capabilities are to be incorporated in future missions (Paul et al. 2011; Roming et al. 2012; Produkt et al. 2005; Park et al. 2013). They are expected to enlarge the detection area and/or volume of X-rays and the aperture of UV/optical/IR telescopes, and improve photometric, temporal and spectral sensitivities as well.

The understanding of GRBs and their underlying physics will be aided by multi-wavelength observations in the early emission phase. Hundreds of GRBs with UV/optical light curves have been measured since the discovery of optical afterglow (Costa et al. 1997). The *Swift* spacecraft, the fastest high-sensitivity space observatory for following the UV/optical afterglow, has simultaneously measured X-ray and UV/optical signals in hundreds of GRBs (Park et al. 2013). However, after nearly 8 years of operation of *Swift*, the immediate aftermath of the explosion is scarcely observed in the optical or UV, because the *Swift* instrument typically responds in ~ 100 s or more. Ground-based telescopes do occasionally respond faster, but to date, only a relatively small number of rapid detections have been produced with heterogeneous sensitivities and other characteristics. Only a few short duration GRBs have been detected in the UV/optical/IR within the first minute after the gamma ray signal.

This lack of early observations and the blindness to the rise phase of many GRB optical light curves along with those of other rapidly variable transient sources leaves fertile astrophysical territory. Many important physical questions arising at short time scales remain unexplored. Rapid data collection is also essential for tests of fundamental physics such as constraints on Lorentz violations (Ellis et al. 2006) and CPT (Kostelecky and Mewes 2008) from the time delay between different energy photons, or between photons and neutrinos. Coincident or successive observations of the explosion event as an electromagnetic counterpart to a neutrino observatory or gravitational wave observatory signal would revolutionize astronomy, and greatly improve our understanding of black holes, neutron stars, and strong field gravity.

The *Swift* observatory obtains UV/optical light curves by first serendipitously detecting the onset of a GRB within the very large field of the Burst Alert Telescope (BAT) (Gehrels et al. 2004). The BAT then produces a crude sky position via a standard coded mask technique. After this, the entire observatory spacecraft slews to point the UV/optical telescope (UVOT) and other instruments at the GRB position. After slewing, a period of time is required for the pointing to stabilize, after which a series of UVOT exposures begins. Though this system has been a great success by producing numerous detections of optical afterglows associated with GRB, only a handful of responses have occurred in less than 60 seconds.

The position calculated by *Swift* within 5–7 s is also broadcast over the Internet via the gamma-ray coordinate network (GCN). At this point, any instrument may respond and follow up the coordinates in the easily-machine-readable format of the GCN alerts, via email or socket connection. Although the response of some instruments on ground (to name a few: ROTSE-I-III, RAPTOR, PAIRTEL, Super-LOTIS, BOOTES) is extremely rapid, e.g. 25 s for ROTSE-III), the sensitivity is far less than that of the *Swift* UVOT. Due to their small size and the limitations of ground-based observations including daytime and weather, these instruments have managed only a handful of rapid detections. A concurrent optical and gamma observation of the prompt phase of GRB080319B was achieved by TORTORA on

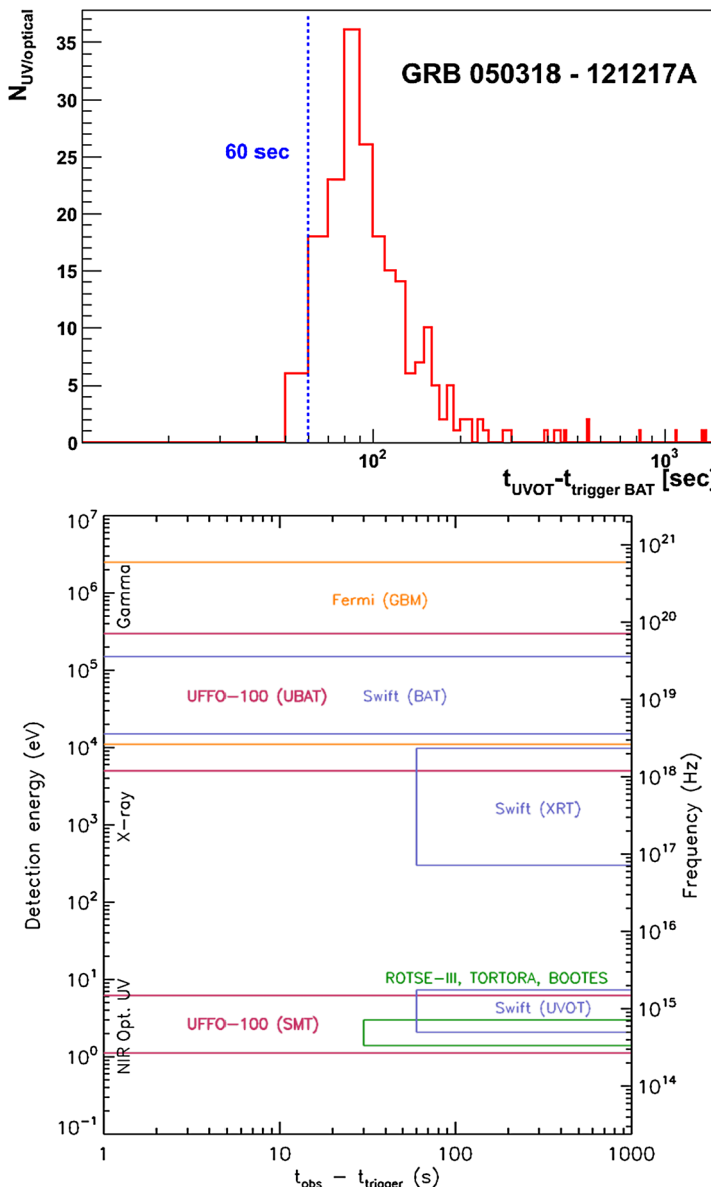


Fig. 16 The domain of frequency and time accessible by space and ground-based experiments. The UFFO missions will explore the fast- and ultra-fast regimes below 60 s and even below 1 s, in a systematic survey

the REM telescope and by ‘π of the Sky’ when this GRB occurred in their field of view and in the field of view of the Konus/Wind instrument. Figure 16 shows the domain of frequency and time accessible by space and ground experiments. The UFFO missions will explore the blank parameter space, the fast- and ultra-fast regimes below 60 sec and even below 1 sec, in a systematic survey and thus significantly enlarge the sample of such observations. Table 1 lists the capability of UV/optical/IR and X-ray observations and the number of events per year for various space missions including two UFFO missions.

Table 1 Major parameters in X-ray/UV/optical observations for various space missions including UFFO/Lomonosov (Park et al. 2013)

| Space mission | BATSE/CGRO (Fishman 1994) | BeppeSAX (Boella et al. 1997) | HETE-2 (Ricker et al. 2002) | Swift (Gehrels et al. 2004) | GBM/Fermi (Perna et al. 2003) | UFFO/Lomonosov |
|-------------------------|--------------------------------|----------------------------------|--|--|----------------------------------|---|
| X-ray | Energy range Detector type | 20 keV–8 MeV NaI(Tl) | 2–30 keV coded mask + proportional counter | 2–25 keV coded mask + proportional counter | 15–150 keV coded mask + CZT | 8 keV–40 MeV NaI + BGO coded mask + YSO |
| Detection area | 8 × 126 cm ² | 140 cm ² | 350 cm ² | 5,240 cm ² | 14 × 126 cm ² | 191 cm ² |
| FOV (half coded) | 4π sr | 40 × 40 deg ² | 80 × 80 deg ² | 100 × 60 deg ² | 2.5 sr | 70.4 × 70.4 deg ² |
| Localization accuracy | ~2 arcdeg in 68% | < 5 arcmin (~1.5 in 99%) | 10 arcmin in 90% | 1–4 arcmin (4 in 8σ) | 1–5 arcdeg | 10 arcmin in 7σ |
| UV/optical | Telescope | None | None | 30 cm φ | None | 10 cm φ |
| | | | | UV/optical | UV/optical | Ritchev-Chrétiens |
| | Response time after trigger | Not applicable | Not applicable | 60 sec | Not applicable | 1 sec |
| GRB events/year | ~300 | ~10 | ~12 | ~100 | ~260 | ~20 |
| Launch-termination year | 1991–2000 | 1996–2002 | 2000–2006 | 2004– | 2008– | 2016– |

Because of the ability of space-based telescopes to detect photons throughout the UV/optical band without atmospheric scattering or absorption, the 30 cm aperture UVOT telescope compares favorably in sensitivity to a 4-m ground-based telescope, and such telescopes are not capable of sub-minute response. The slower slew times of such larger terrestrial telescopes makes them uncompetitive for the sub-1000 sec regime. The *Swift* limit of 60 s response is therefore the practical minimum for sensitive UV/optical GRB studies for the near to mid-term future. In the following we propose a new technical solution to overcome the constraints of current instrumentation.

4.2 Method of Measurements

The objective of GRB studies during the Lomonosov mission is to accomplish simultaneous burst detections within the X-ray/gamma-ray and UV/optical ranges along with the possibility of prompt emission as well as obtaining precursor light curves. This possibility provides unique information about GRB central engine functioning.

Successful detections of optical emissions simultaneously with the prompt γ -ray emission have proven to be rare since the discovery of the first such coincidence in January 1999 by ROTSE (Robotic Optical Transient Search Experiment) (Akerlof et al. 1999). Although the discovery is 16 years old, fewer than twenty successful optical observations coincident or close-to-coincident with the gamma-ray burst have been made so far, and fewer than ten of them are suitable for our analysis. This is in sharp contrast to the power-low tail of the optical and x-ray afterglow, which has been observed several hundred times. The reason is that GRBs usually last no longer than a few tens or hundreds of seconds. Consequently, prompt and early optical emissions of a GRB are much harder to observe than the afterglow.

It has already been pointed out (Vestrand et al. 2005) that two types of the behavior of optical flux of gamma-ray bursts are observed. In the first case, the optical emission appears simultaneously and correlates with the gamma-ray emission (GRB080319B, GRB100901A). In the second case, the optical emission appears before the very end or even after the end of the gamma-ray burst and varies very smoothly: it first increases, reaches a maximum, and then gradually fades into the afterglow.

In this way, we plan to use successive experience of ground-based systems of wide field cameras and robotic telescopes of MASTER Global Robotic Net (Lipunov et al. 2010; Kornilov et al. 2012), which had detected the prompt emission of several GRBs (Gorbovskoy et al. 2011, 2016; Tyurina et al. 2010).

The key aspect for the Lomonosov mission to achieve its objective in GRB observation is to utilize the co-aligned system of X-ray/gamma-ray and UV/optical detectors for simultaneous burst detections in X-ray/gamma-ray and optical ranges. There are two such co-aligned systems in the Lomonosov mission as stated in the beginning of Sect. 4.

One of the two co-aligned systems is the BDRG plus SHOK system. The BDRG detector consists of three crystal scintillators arranged orthogonally. Each crystal scintillator has an active area of 120 cm^2 and covers the X-ray/gamma-ray energy range of 0.01 to 3.0 MeV. The BDRG detector has the field of view (FOV) of $2\pi \text{ sr}$ and it is capable of triggering (i.e. localizing) X-ray/gamma-ray sources in the sky with an accuracy of 1 to 4 degrees. The SHOK detector consists of a pair of optical cameras with stationary super-wide FOV. Each camera has a FOV of about $1,000 \text{ deg}^2$. The maximum frame rate of the SHOK is 5–7 frames per second and the image data are continuously stored on board for a specific period of time before being overwritten. In case that a trigger for a X-ray/gamma-ray source occurs, all SHOK image data from one minute before till two minutes after the trigger will be transmitted to the ground station. In this system, the FOV of the SHOK will be inside

the FOV of the BDGR and it will not be necessary to redirect the SHOK. Thus, there is no time gap between UV/optical and X-ray/gamma-ray signals, and even the signals prior to the trigger (including the possible precursor signals) are recorded.

The other of the two co-aligned systems is the UFFO which consists of the X-ray telescope UBAT and the Ritchey-Chretien UV/optical telescope SMT. The UBAT has a coded mask and an array of YSO (Y_2SiO_5) crystal scintillators to trigger X-ray/gamma-ray sources. The half-coded FOV of the UBAT is $70.4 \times 70.4 \text{ deg}^2$ and its sensitive energy range for detecting X-rays/gamma-rays is from 5 to 150 keV. The localization accuracy of the UBAT is 10 arcmin. The Ritchey-Chretien telescope SMT is a 10 cm diameter aperture modified Ritchey-Chretien telescope equipped with a reflector of 15 cm diameter flat mirror that is rotated towards any light source within solid angle view of 70×70 less than a second after receiving the trigger from the UBAT. The focal plane detector of the SMT is an Intensified Charge-Coupled Device (ICCD) which consists of 256×256 monochromic pixels with a pixel FOV of $4 \times 4 \text{ arcsec}^2$. So the FOV of the SMT is $17 \times 17 \text{ arcmin}^2$ which is wide enough to contain a potential GRB triggered by the UBAT. The adoption of a very fast rotating mirror for the UV/optical detection upon a trigger from the X-ray/gamma-ray detection in the UBAT plus SMT system is an innovative approach that can achieve a good spatial resolution in the UV/optical detection with minimal loss in the temporal information.

Finally it is worth for one co-aligned system to carry out its UV/optical detection using the cross-over trigger from the other co-aligned system even though the chance of a GRB event occurring in the overlapped area in the FOVs of two such co-aligned systems is small.

5 Near-Earth Radiation Environment

Since the discovery of the Van Allen electron radiation belts by the first US and Soviet missions over 50 years ago, scientists have made significant progress in understanding physics of the radiation belts. Understanding of relativistic electron dynamics is most important for the understanding of deep dielectric chagrin. As relativistic electrons lead to differential internal charging and may lead to anomalies or failure of the critical electronics on board of the spacecraft.

Since the launch of Van Allen Probes mission in 2012 radiation belt research has focused on identifying the energization mechanisms responsible for acceleration to MeV energies and above MeV. However, the complicated dynamical response of the radiation belts depends not only on acceleration but also on loss processes. Reeves et al. (2003) found that geomagnetic storms can increase (A), significantly decrease (B), or not substantially change (C) the fluxes of relativistic electrons during storms (Fig. 17). The statistical analysis of Reeves et al. (2003) showed that the probability of each scenario is 53, 19, and 28% for scenarios A, B, and C, respectively.

The differences in the responses of radiation belts to storms are due to competition between various acceleration and loss processes (e.g. Shprits et al. 2008a, 2008b). While Van Allen Probes mission and Time History of Events and Macroscale Interactions during Substorms (THEMIS) mission have near-equatorial orbits, which are optimal for evaluating the acceleration of trapped electrons, there is currently no mission that allows to observe precipitating fluxes and clearly separate them from trapped fluxes.

Radiation belt investigations on Lomonosov will be able to address the following scientific questions:

What physical mechanisms lead to particle precipitation from the Earth's radiation belts, under the quiet and disturbed geomagnetic conditions?

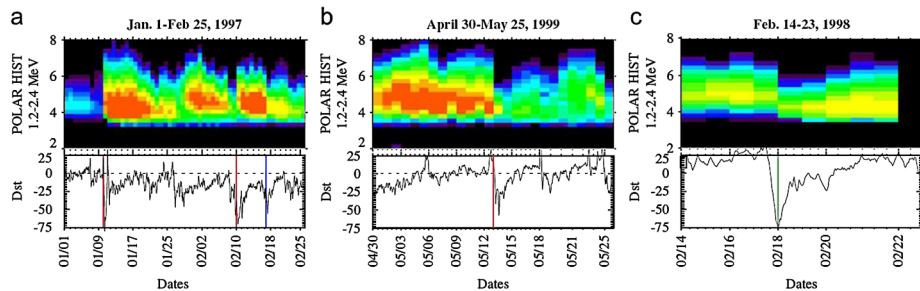


Fig. 17 Details of the three types of responses. (a) A strong increase in relativistic electron fluxes in response to the January 1997 geomagnetic storm. (b) A dramatic and permanent loss of electrons throughout the outer belt in May 1999. (c) A 100 nT storm in February 1998 with peak fluxes after the storm very similar to those before the storm (Reeves et al. 2003)

How does precipitation of the magnetospheric particles penetrating into the atmosphere cause local and wide-scale ionospheric disturbances, ozone layer variations and atmospheric ionization?

What are the conditions in the solar wind and magnetosphere that can lead to dangers increase in radiation at LEO orbit?

The narrow field of ELFIN-L particle instruments will allow to resolve the loss cone and quantify fluxes of the precipitating electrons. Together will equatorial measurements we will be able to quantify the acceleration and loss of particles from the belts which will help understand the competition between acceleration and loss. Measurements of the energy spectrum and pitch angle distribution of electrons will allow us to differentiate between the loss due to chorus wave and loss due to EMIC waves, while measurements provided by UCLA PRM magnetometer will help determine the pitch angles observed by the instrument.

Thus, the design of the instrument DEPRON (Dosimeter of Electrons, PROtons and Neutrons) was determined. DEPRON is intended for registration of the absorbed doses and linear energy transfer spectra for high-energy electrons, protons and nuclei of space radiation, as well as registration of thermal and slow neutrons. The experiment based on the DEPRON instrument is aimed at the studies of the distribution of space radiation doses at a rate of high latitude paths in order to study the conditions of perspective-manned spacecraft.

6 Experiment for Recording and Analysis of Accelerations in Orbital Flight

The purposes of the analysis of acceleration in orbital flight concern the field of biophysics and human physiology. They are closely associated with so-called “space motion sickness,” which, in particular, manifests itself as gaze stabilization delay (Kornilova et al. 2006; Tomilovskaya and Kozlovskaya 2010). Both Russian scientists and NASA experts have confirmed this fact many times. Due to this delay, visual control of the moving objects becomes more complicated, and its quality decreases (Sadovnichiy et al. 2010). In order to estimate the quality of the visual control of the moving objects, one can use, for instance, maximum quality testing method (Sadovnichiy et al. 2015; Aleksandrov et al. 2015).

A gaze stabilization corrector is developed for protection against the described phenomenon. One of the assumptions explaining the reasons of “motion sickness” is based

Table 2 BI parameters

| Parameter, units | Value |
|--|----------------|
| Data exchange rate, (Ethernet line), Gbit/s | 1 |
| Command/data exchange rate, (CAN bus), Mbit/s | 1 |
| Command exchange rate, (MIL-STD-1553B bus), Mbit/s | 1 |
| Data transmitting rate, (LVDS bus), Mbit/s | 16 |
| Mass, kg | 8.5 |
| Power consumption, Watt | |
| max | 31 |
| min | 16 |
| Voltage, V | 27^{+7}_{-4} |
| Data volume without redundancy, GByte | 512 |

on the vestibulosensory nonconformity of information coming to the central nervous system from two types of vestibular sensors—semicircular canals and otolith organs, which appear in space. Conforming information is regarded as a set of signals, coming from the lateral semicircular canals and from the inertial mechanoreceptors of the otolith organs, which are sensitive to the existence of gravity force at a vertical position. In a zero-gravity state, there are no signals from the mechanoreceptors, and it leads to nonconformity. As a result of this nonconformity, the cerebellar switches off feedback between the ocular movement control center and vestibular system, and it leads to the increase of the gaze stabilization delay. It is expected that the corrector will defuse this conflict and diminish gaze stabilization delay. It is supposed that the effect will be achieved by means of forming a signal consisting of two components. One of them will informationally simulate gravity force on orbit (it will diminish nonconformity of the information coming from semicircular canals and otolith organs), and the second will enhance the role of the signals on the angular movement of the cosmonaut's head (Sadovnichii et al. 2013). The corrector will convey the signals by means of galvanic vestibular stimulation.

7 Instrumental Complex and Onboard Data Acquisition

The data from all scientific instruments, i.e. TUS, BDRG, SHOK, UFFO, ELLIN-L, DEPRON and IMISS-1 are stored in the special “Information unit” BI (Block of Information). It also provides control of the scientific instruments as well as transmitting scientific and telemetric data to the Earth. All instruments are connected with BI according to the wire-diagram presented in Fig. 19.

BI parameters are given in Table 2.

BI is made as a monoblock, though it consists of two identical parts. When one part operates, the other stays in cold reserve. All the data and power lines have dual redundancy. BI uses MIL-STD-1553B as the command line, CAN, Ethernet, and RS232 buses to connect to other scientific instruments, LVDS line to send data to the radiolink.

The scientific instruments and BI connections are shown in Fig. 18.

The main operational mode of BI is continuous monitoring of payload instruments status including its self-diagnosis, new data uploading from other instruments, the reception of GCC commands, telemetry and data exchange with the bus, and payload data download to the Earth.

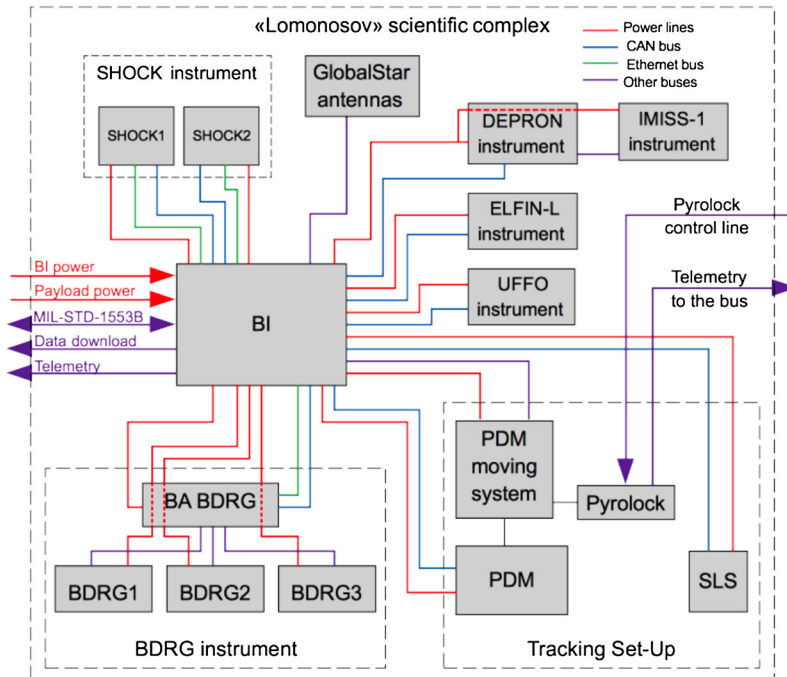


Fig. 18 Scientific complex structure

The BI wire-diagram is presented in Fig. 19. It consists of 11 units:

- Processor unit;
- MIL-STD-1553B bus unit;
- CAN bus unit;
- Payload data download unit;
- BI power supply unit;
- Payload power supply unit;
- Ethernet commutation unit;
- 1-wire bus unit;
- GlobalStar modem unit;
- Analog telemetry unit; and
- Data storage unit.

The processor unit controls all other BI units as well as scientific instruments. It provides all necessary calculations, data packing/unpacking, commands execution, etc. It runs on the Linux Debian operating system (OS). The onboard clock accuracy is 3 seconds per day, but it is also been synchronized with a satellite clock once per hour and each time BI is turned on. BI distributes a time marker between all scientific devices every time after synchronization with the satellite bus. BI also obtains information about orientation and navigation of the satellite, each second. This information is used for calculating the detector’s field of view orientation.

The MIL-STD-1553B unit has two independent lines for main and reserve BI parts to connect to the spacecraft bus. Each line has a 1 Mbit/s transfer rate. Lines could be hot swapped without working mode termination. The bus bandwidth is 1 Mbit per second.

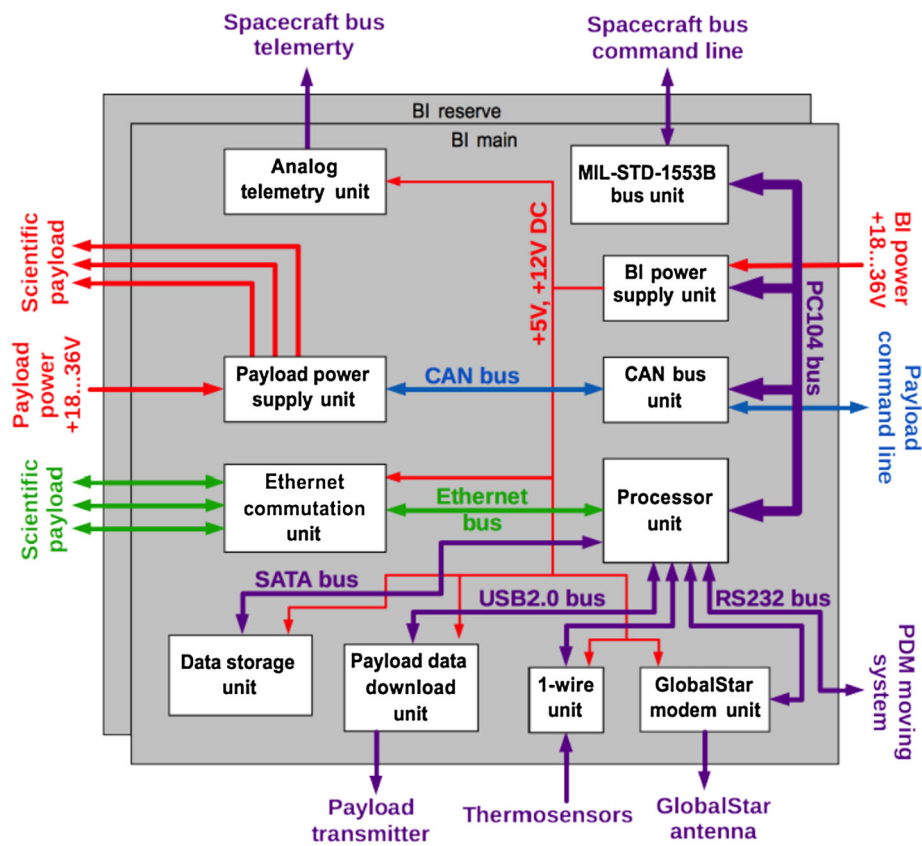


Fig. 19 BI wire-diagram

The Ethernet commutation unit is a Gigabit Ethernet switch. It allows uploading of large amounts of scientific data from SHOK and BDRG instruments on high speed. It is also used as testing interface during ground testing.

The CAN bus unit has two independent CAN lines, one of which is used for payload power management, and the other as a main command line of the scientific complex. DEPRON, ELFIN-L, UFFO and TUS detector have rather small data rate, thus they also use CAN bus to download data to BI. The CAN bus bandwidth is 1 Mbit per second.

The BI power supply unit powers all the units inside BI with stabilized +5 and +12 V DC. It runs on input 18 to 36 V DC, and its noise reduction system allows fulfilling the Electromagnetic Compatibility requirements.

The payload power supply unit manages other instruments' power supply including commutation, line protection from shortcuts and increased power consumption. It also monitors input voltage level, currents and temperatures.

The analog telemetry unit sends to the spacecraft bus information about BI and payload power status for both main and reserve semi-kits.

The data storage unit consists of two SSDs with a total volume of 512 GBytes per semi-kit. Scientific data is stored in ring buffers. The data storage unit also keeps the last 20 scientific data download sessions.

Summary memory volume for payload scientific data is 512 Gbyte for one BI semi-kit. Approximate quotation for storing scientific payload data is as follows:

- telemetry data and housekeeping from payload including BI: ~ 100 MBt/day;
- scientific data from BDRG: ~ 300 MBt/day;
- scientific data from SHOK cameras: < 1.1 GBt/day for each camera;
- scientific data from UFFO: < 300 MBt/day;
- scientific data from DEPRON: ~ 10 MBt/day;
- scientific data from IMISS-1: < 10 MBt/day;
- scientific data from TUS: ~ 150 MBt/day;
- scientific data from ELFIN-L: < 100 MBt/day;
- telemetry data and housekeeping from TUS: < 5 MBt/day.

The volume of service telemetry data received from board is 10 MBt/day.

The life of data memory cells is 10^6 rewrite cycles that corresponds to 5 years of continuous work.

1-wire unit provides connection of the set of digital thermosensors which are used for the inner housekeeping information of scientific complex. GlobalStar unit provides the fast GRB trigger transmission to the Earth using the GlobalStar satellite system.

Payload data download unit links BI with the payload information transmitter, providing the stored data transmission to the ground. The unit interface is of the LVDS type; it has dual redundancy, and the data rate for each channel is 61.44 Mbit/s.

One of the most important scientific goals is to transmit new GRB alerts to the ground observation network. The GlobalStar communication system is intended to solve this problem. It could also be used as a reserve channel of scientific payload telemetry transmitting. According to calculations, the coverage of the Lomonosov spacecraft orbit by the GlobalStar system is about 86% (taking into account antenna orientation). If the satellite flies over the GlobalStar coverage area during the GRB detection, the time interval from event registration to trigger receipt on the ground is an average of 2.5 s in the case of open connection with the server, and up to 40–60 s connection is closed or server is busy. Message contains a GRB coordinate error box, which could become more accurate during the event registration process. Besides, payload telemetry data sample and the truncated scientific data set are also being transmitted to the Earth via GlobalStar for operative monitoring of instrument status. The volume of transmitted additional data could be changed, depending on the volume of the main GRB data. On the other hand, additional calibration parameters (if present), firmware software and other operative data could be transmitted from the ground via GlobalStar.

There is a built-in self-testing system, which operates in BI continuously. Operation of all units is checked regularly using internal self-diagnostic algorithms. The scientific and telemetry data as well as BI status flags are recorded on SSD in the BI storage unit, which is also being checked by an internal S.M.A.R.T. (self-monitoring, analysis and reporting technology) system.

The main goal of the BI operation is maximum possible autonomy of the scientific complex and minimum use of manual control.

8 Conclusion

Scientific complexes installed onboard the Lomonosov satellite provide studies of a wide range of problems in modern astrophysics and space physics, mainly the studies of extreme events in sources placed on cosmological distances such as UHECR and GRB. The Lomonosov mission provides opportunities for solving the aforementioned problems.

Scientific payload of the Lomonosov satellite will include a complex of instruments for studying the processes of charged particle penetration into the upper atmosphere of the Earth and for the analysis of the radiation conditions at low altitudes. Another task is the study of registration of angular and linear accelerations acting on sensitive mass in terms of near-Earth orbital flight.

The scientific equipment installed onboard the Lomonosov satellite includes the number of instruments intended for solving scientific problems mentioned above:

- An optical wide aperture telescope TUS for imaging of the UHECR tracks in the atmosphere;
- A set of instruments for GRB study including gamma-ray monitor BDRG, optical wide-field cameras SHOK, and UFFO instruments consisting of UV and X-ray telescopes;
- A set of instruments studying the energetic particle fluxes in the near-Earth space including magnetometer, high-energy electron detector ELFIN-L and charge and neutral particle monitor DEPRON; and
- The IMISS-1 instrument for recording and analysis of accelerations in orbital flight.

In the following papers of this issue, we present more detailed reviews of the scientific problems, i.e. UHECR, GRB, TLE and magnetosphere relativistic electrons in view of the Lomonosov mission scientific objectives, as well as scientific instruments and methods for TUS, BDRG, SHOK, UFFO, ELFIN-L, DEPRON and IMISS-1.

Acknowledgements Scientific experiments onboard the Lomonosov satellite are realized with the financial support of M.V. Lomonosov Moscow State University within the framework of the “Prospects for Development” program (“Perspektivnye Napravleniya Razvitiya”). The TUS instrument was manufactured in the frame of the Russian Space program with financial support from the Russian Space Agency (Roscosmos). Korean group was supported by the National Research Foundation grants (No. 2015R1A2A1A01006870, and No. 2015R1A2A1A15055344). All authors thank the employees of JSC VNIIM for successful cooperation in the development and manufacture service platform of the satellite Lomonosov and ensuring quality of information transmission the data of a scientific complex of instruments.

Open Access This article is distributed under the terms of the Creative Commons Attribution 4.0 International License (<http://creativecommons.org/licenses/by/4.0/>), which permits unrestricted use, distribution, and reproduction in any medium, provided you give appropriate credit to the original author(s) and the source, provide a link to the Creative Commons license, and indicate if changes were made.

References

- A. Aab, P. Abreu, M. Aglietta et al., Depth of maximum of airshower profiles at the Pierre Auger Observatory. I. Measurements at energies above $10^{17.8}$ eV. *Phys. Rev. D* **90**(12), 122005 (2014a). doi:[10.1103/PhysRevD.90.122005](https://doi.org/10.1103/PhysRevD.90.122005)
- A. Aab, P. Abreu, M. Aglietta et al., Depth of maximum of airshower profiles at the Pierre Auger Observatory. II. Composition implications. *Phys. Rev. D* **90**(12), 122006 (2014b). doi:[10.1103/PhysRevD.90.122006](https://doi.org/10.1103/PhysRevD.90.122006)
- A. Aab, P. Abreu, M. Aglietta et al., Searches for large-scale anisotropy in the arrival directions of cosmic rays detected above energy of 10^{19} eV at the Pierre Auger Observatory and the Telescope Array. *Astrophys. J.* **794**, 172 (2014c). doi:[10.1088/0004-637X/794/2/172](https://doi.org/10.1088/0004-637X/794/2/172)
- A. Aab, P. Abreu, M. Aglietta et al., Large scale distribution of ultra high energy cosmic rays detected at the Pierre Auger Observatory with zenith angles up to 80° . *Astrophys. J.* **802**, 111 (2015a). doi:[10.1088/0004-637X/802/2/111](https://doi.org/10.1088/0004-637X/802/2/111)
- A. Aab, P. Abreu, M. Aglietta et al., Searches for anisotropies in the arrival directions of the highest energy cosmic rays detected by the Pierre Auger Observatory. *Astrophys. J.* **804**, 15 (2015b). doi:[10.1088/0004-637X/804/1/15](https://doi.org/10.1088/0004-637X/804/1/15)
- A. Aab, P. Abreu, M. Aglietta et al., The Pierre Auger Cosmic Ray Observatory. *Nucl. Instrum. Methods Phys. Res., Sect. A, Accel. Spectrom. Detect. Assoc. Equip.* **798**, 172–213 (2015c). doi:[10.1016/j.nima.2015.06.058](https://doi.org/10.1016/j.nima.2015.06.058)

R.U. Abbasi, T. Abu-Zayyad, M. Allen et al., First observation of the Greisen-Zatsepin-Kuzmin suppression. *Phys. Rev. Lett.* **100**(10), 101101 (2008). doi:[10.1103/PhysRevLett.100.101101](https://doi.org/10.1103/PhysRevLett.100.101101)

R.U. Abbasi, M. Abe, T. Abu-Zayyad et al., Indications of intermediate-scale anisotropy of cosmic rays with energy greater than 57 EeV in the Northern sky measured with the surface detector of the Telescope Array experiment. *Astrophys. J. Lett.* **790**, 21 (2014). doi:[10.1088/20418205/790/2/L21](https://doi.org/10.1088/20418205/790/2/L21)

R.U. Abbasi, M. Abe, T. Abu-Zayyad et al., Study of ultra-high energy cosmic ray composition using Telescope Array’s middle drum detector and surface array in hybrid mode. *Astropart. Phys.* **64**, 49–62 (2015a). doi:[10.1016/j.astropartphys.2014.11.004](https://doi.org/10.1016/j.astropartphys.2014.11.004)

R.U. Abbasi, J. Bellido, J. Belz et al., Report of the working group on the composition of ultra high energy cosmic rays. (2015b). [arXiv:1503.07540](https://arxiv.org/abs/1503.07540)

B.P. Abbott et al., *Phys. Rev. Lett.* **116**, 061102 (2016a)

B.P. Abbott et al., *Phys. Rev. X* **6**, 041015 (2016b)

J. Abraham et al., *Nucl. Instrum. Methods Phys. Res., Sect. A, Accel. Spectrom. Detect. Assoc. Equip.* **523**, 50 (2004). <http://www.auger.org>

J. Abraham, P. Abreu, M. Aglietta et al., Correlation of the highest-energy cosmic rays with nearby extragalactic objects. *Science* **318**, 938–943 (2007). doi:[10.1126/science.1151124](https://doi.org/10.1126/science.1151124)

J. Abraham, P. Abreu, M. Aglietta et al., Correlation of the highest-energy cosmic rays with the positions of nearby active galactic nuclei. *Astropart. Phys.* **29**, 188–204 (2008a). doi:[10.1016/j.astropartphys.2008.01.002](https://doi.org/10.1016/j.astropartphys.2008.01.002)

J. Abraham, P. Abreu, M. Aglietta et al., Observation of the suppression of the flux of cosmic rays above 4×10^{19} eV. *Phys. Rev. Lett.* **101**(6), 061101 (2008b). doi:[10.1103/PhysRevLett.101.061101](https://doi.org/10.1103/PhysRevLett.101.061101)

A. Abramovici et al., *Science* **256**, 325 (1992). <http://www.ligo.caltech.edu>

P. Abreu, M. Aglietta, E.J. Ahn et al., Update on the correlation of the highest energy cosmic rays with nearby extragalactic matter. *Astropart. Phys.* **34**, 314–326 (2010). doi:[10.1016/j.astropartphys.2010.08.010](https://doi.org/10.1016/j.astropartphys.2010.08.010)

T. Abu-Zayyad et al., *Nucl. Instrum. Methods Phys. Res., Sect. A, Accel. Spectrom. Detect. Assoc. Equip.* **689**, 87 (2012)

T. Abu-Zayyad, R. Aida, M. Allen et al., Correlations of the arrival directions of ultra-high energy cosmic rays with extragalactic objects as observed by the Telescope Array experiment. *Astrophys. J.* **777**, 88 (2013a). doi:[10.1088/0004-637X/777/2/88](https://doi.org/10.1088/0004-637X/777/2/88)

T. Abu-Zayyad, R. Aida, M. Allen et al., The cosmic-ray energy spectrum observed with the surface detector of the Telescope Array experiment. *Astrophys. J. Lett.* **768**, 1 (2013b). doi:[10.1088/2041-8205/768/1/L1](https://doi.org/10.1088/2041-8205/768/1/L1)

J.H. Adams, S. Ahmad, J.-N. Albert et al., An evaluation of the exposure in nadir observation of the JEM-EUSO mission. *Astropart. Phys.* **44**, 76–90 (2013). doi:[10.1016/j.astropartphys.2013.01.008](https://doi.org/10.1016/j.astropartphys.2013.01.008)

C. Akerlof et al., *Nature* **398**, 400 (1999)

I. Al Samarai, Indications of anisotropy at large angular scales in the arrival directions of cosmic rays detected at the Pierre Auger Observatory, in *Proceedings of Science (ICRC2015)* (2015), p. 372

V.V. Aleksandrov, T.B. Alexandrova, E. Soto et al., An output signal correction algorithm for vestibular mechanoreceptors to simulate passive turns. *Mosc. Univ. Mech. Bull.* **70**(5), 130–134 (2015)

L. Amati et al., *Mon. Not. R. Astron. Soc.* **391**, 577 (2008)

D.R. Bergman (High Resolution Fly’s Eye Collaboration), Observation of the GZK cutoff using the HiRes detector. *Nucl. Phys. B, Proc. Suppl.* **165**, 19–26 (2007). doi:[10.1016/j.nuclphysbps.2006.11.004](https://doi.org/10.1016/j.nuclphysbps.2006.11.004)

M.G. Bernardini, R. Margutti, E. Zaninoni, G. Chincarini, *Mon. Not. R. Astron. Soc.* **425**, 1199 (2012)

G. Boella et al., *Astron. Astrophys. Suppl. Ser.* **122**, 299 (1997). <http://www.asdc.asi.it/bepposax>

V. Bromm, A. Loeb, High-redshift gamma-ray bursts from population III progenitors. *Astrophys. J.* **642**, 382 (2006)

H.J. Christian et al., The lightning imaging sensor, in *11th International Conference on Atmospheric Electricity* (1999), pp. 746–749. (NASA/CP-1999-209261); (SEE 19990108601)

E. Costa et al., *Nature* **387**, 783 (1997)

S.A. Cummer, N. Jaugey, J. Li et al., Submillisecond imaging of sprite development and structure. *Geophys. Res. Lett.* **33**, L04104 (2006). doi:[10.1029/2005GL024969](https://doi.org/10.1029/2005GL024969)

C. Cutler, K.S. Thorne (2002). [arXiv:gr-qc/0204090](https://arxiv.org/abs/gr-qc/0204090)

B.R. Dawson, I.C. Mariş, M. Roth et al., The energy spectrum of cosmic rays at the highest energies, in *European Physical J. Web of Conf.*, vol. 53 (2013), 1005. doi:[10.1051/epjconf/20135301005](https://doi.org/10.1051/epjconf/20135301005)

R.M. de Almeida, Constraints on the origin of cosmic rays from large scale anisotropy searches in data of the Pierre Auger Observatory, in *Proc. 33rd Int. Cosmic Ray Conf.*, Rio de Janeiro (2013)

O. Deligny, Large-scale distribution of arrival directions of cosmic rays detected at the Pierre Auger Observatory and the Telescope Array above 10^{19} eV, in *Proceedings of Science (ICRC2015)* (2015), p. 395

J. Ellis et al., *Astropart. Phys.* **25**, 402 (2006)

G.J. Fishman, *Astrophys. J. Suppl. Ser.* **92**, 229 (1994). <http://heasarc.gsfc.nasa.gov/docs/cgro>

R. Franz, R. Nemzek, J. Winckler, Television image of a large upward electrical discharge above a thunderstorm system. *Science* **249**, 48–51 (1990)

M. Fukushima, Recent results from Telescope Array, in *European Physical Journal Web of Conferences*, vol. 99 (2015), 04004. doi:[10.1051/epjconf/20159904004](https://doi.org/10.1051/epjconf/20159904004)

M. Fukushima, D. Ivanov, E. Kido et al., Search for large-scale anisotropy of ultra-high energy cosmic rays with the Telescope Array, in *Proc. 33rd Int. Cosmic Ray Conf.*, Rio de Janeiro (2013)

G.K. Garipov, B.A. Khrenov, M.I. Panasyuk et al., UV radiation from the atmosphere: results of the MSU “Tatiana” satellite measurements. *Astropart. Phys.* **24**(4–5), 400–408 (2005). doi:[10.1016/j.astropartphys.2005.09.001](https://doi.org/10.1016/j.astropartphys.2005.09.001)

G.K. Garipov, M.I. Panasyuk, I.A. Rubinshtein et al., Ultraviolet radiation detector of the MSU research educational microsatellite Universitetskii-Tatyana. *Instrum. Exp. Tech.* **49**(1), 126–131 (2006). doi:[10.1134/S0020441206010180](https://doi.org/10.1134/S0020441206010180)

G.K. Garipov, P.A. Klimov, V.S. Morozenko et al., Time and energy characteristics of UV flashes in the atmosphere: data of the Universitetsky-Tatiana satellite. *Cosm. Res.* **49**(5), 391–398 (2011). doi:[10.1134/S0010952511050066](https://doi.org/10.1134/S0010952511050066)

G.K. Garipov, B.A. Khrenov, P.A. Klimov et al., Global transients in ultraviolet and red-infrared ranges from data of Universitetsky-Tatiana-2 satellite. *J. Geophys. Res.* **118**(2), 370–379 (2013). doi:[10.1029/2012JD017501](https://doi.org/10.1029/2012JD017501)

N. Gehrels et al., *Astrophys. J.* **611**, 1005 (2004). <http://heasarc.gsfc.nasa.gov/docs/swift/swiftsc.html>

G. Ghirlanda et al., *New J. Phys.* **8**, 123 (2006)

E.S. Gorbovskoy, G.V. Lipunova, V.M. Lipunov, V.G. Kornilov, A.A. Belinski, N.I. Shatskiy, N.V. Tyurina, D.A. Kuvshinov, P.V. Balanutsa, V.V. Chazov, A. Kuznetsov, D.S. Zimnukhov, M.V. Kornilov, A.V. Sankovich, A. Krylov, K.I. Ivanov, O. Chvalae, V.A. Poleschuk, E.N. Konstantinov, O.A. Gress, S.A. Yaze, N.M. Budnev, V.V. Krushinski, I.S. Zalozhni, A.A. Popov, A.G. Tlatov, A.V. Parhomenko, D.V. Dormidontov, V. Senik, V.V. Yurkov, Yu.P. Sergienko, D. Varda, I.P. Kudelina, A.J. Castro-Tirado, J. Gorosabel, R. Sánchez-Ramírez, M. Jelinek, J.C. Tello, Prompt, early, and afterglow optical observations of five gamma-ray bursts (GRBs 100901A, 100902A, 100905A, 100906A, and 101020A). *Mon. Not. R. Astron. Soc.* **421**(3), 1874–1890 (2011)

E.S. Gorbovskoy, V.M. Lipunov, D.A.H. Buckley, V.G. Kornilov, P.V. Balanutsa, N.V. Tyurina, A.S. Kuznetsov, D.A. Kuvshinov, I.A. Gorbunov, D. Vlasenko, E. Popova, V.V. Chazov, S. Potter, M. Kotze, A.Y. Kniazev, O.A. Gress, N.M. Budnev, K.I. Ivanov, S.A. Yaze, A.G. Tlatov, V.A. Senik, D.V. Dormidontov, A.V. Parhomenko, V.V. Krushinski, I.S. Zalozhni, R.A. Castro-Tirado, R. Sánchez-Ramírez, Yu.P. Sergienko, A. Gabovich, V.V. Yurkov, H. Levato, C. Saffe, C. Mallamaci, C. Lopez, F. Podest, V.V. Vladimirov, *Mon. Not. R. Astron. Soc.* **455**(3), 3312–3318 (2016). <http://adsabs.harvard.edu/abs/2016MNRAS.455.3312G>

P.W. Gorham et al., *Astropart. Phys.* **32**, 10 (2009). <http://www.ps.uci.edu/~anita/index.html>

J. Greiner et al., *Astron. Astrophys.* **526**, 10 (2011)

K. Greisen, End to the cosmic-ray spectrum? *Phys. Rev. Lett.* **16**, 748–750 (1966). doi:[10.1103/PhysRevLett.16.748](https://doi.org/10.1103/PhysRevLett.16.748)

F. Halzen, S.R. Klein, *Rev. Sci. Instrum.* **81**, 081101 (2010). <http://icecube.wisc.edu>

W. Hanlon, D. Ikeda, Energy spectrum and mass composition of ultrahigh energy cosmic rays measured by the hybrid technique in Telescope Array, in *Proceedings of Science (ICRC2015)* (2015), p. 362

D. Harari, The flux suppression at the highest energies. *C. R. Phys.* **15**(4), 376–383 (2014). doi:[10.1016/j.crhy.2014.02.011](https://doi.org/10.1016/j.crhy.2014.02.011)

D. Ivanov, TA spectrum summary, in *Proceedings of Science (ICRC2015)* (2015), p. 349

S. Jeong et al., *Opt. Express* **21**(2), 2263 (2013)

K. Kawata, M. Fukushima, D. Ikeda et al., Ultra-high-energy cosmic-ray hotspot observed with the Telescope Array surface detector, in *Proceedings of Science (ICRC2015)* (2015), p. 276

B.A. Khrenov, M.I. Panasyuk, V.V. Alexandrov et al., *AIP Conf. Proc.* **566**, 5 (2001)

M.D. Kistler et al., The star formation rate in the reionization era as indicated by gamma-ray bursts. *Astrophys. J.* **705**, L104 (2009)

P.A. Klimov, M.I. Panasyuk, B.A. Khrenov, G.K. Garipov, N.N. Kalmykov, V.S. Morozenko, V.L. Petrov, S.A. Sharakin, A.V. Shirokov, I.V. Yashin, M.Y. Zotov, S.V. Biktemerova, A.A. Grinyuk, V.M. Grebenyuk, M.V. Lavrova, L.G. Tkachev, A.V. Tkachenko, I.H. Park, J. Lee, S. Jeong, O. Martinez, H. Salazar, E. Ponce, O.A. Saprykin, A.A. Botvinko, A.N. Senkovsky, A.E. Puchkov, Space experiment TUS on board the Lomonosov satellite. *Space Sci. Rev.* (2017, this issue)

D. Kocevski, *Astrophys. J.* **747**, 146 (2012)

V. Kornilov, V. Lipunov, E. Gorbovskoy, A. Belinski, D. Kuvshinov, N. Tyurina, N. Shatsky, A. Sankovich, A. Krylov, P. Balanutsa, V. Chazov, A. Kuznetsov, D. Zimnukhov, V. Senik, A. Tlatov, A. Parkhomenko, D. Dormidontov, V. Krushinsky, I. Zalozhnyh, A. Popov, S. Yaze, N. Budnev, K. Ivanov, E. Konstantinov, O. Gress, O. Chvalae, V. Yurkov, Yu. Sergienko, I. Kudelina, Robotic optical telescopes global network MASTER II. Equipment, structure, algorithms. *Exp. Astron.* **33**(1), 173–196 (2012)

L.N. Kornilova, M.I. Alekhina, V.V. Temnikova, S.V. Sagalovich, S.V. Malakhov, I.A. Naumov, I.B. Kozlovskaya, M. Reshke, A.V. Vasin, The effect of a long stay under microgravity in the vestibular function and tracking eye movements. *Hum. Physiol.* **32**(5), 547–555 (2006)

V.A. Kostelecky, M. Mewes, *Astrophys. J.* **689**, L1 (2008)

C.-L. Kuo, A.B. Chen et al., Modeling elvés observed by FORMOSAT-2 satellite. *J. Geophys. Res.* **112**, A11312 (2007). doi:10.1029/2007JA012407

D.Q. Lamb, D.E. Reichart, Gamma-ray bursts as a probe of the very high redshift universe. *Astrophys. J.* **536**, 1 (2000)

J. Linsley, Evidence for a primary cosmic-ray particle with energy 10^{20} eV. *Phys. Rev. Lett.* **10**, 146–148 (1963). doi:10.1103/PhysRevLett.10.146

J. Linsley, R. Benson, in *Proc. of the 17th ICRC*, Paris, vol. 8 (1981), p. 145

J. Linsley, L. Scarsi, B. Rossi, Extremely energetic cosmic-ray event. *Phys. Rev. Lett.* **6**, 485–487 (1961). doi:10.1103/PhysRevLett.6.485

V. Lipunov, V. Kornilov, E. Gorbovskoy, N. Shatskij, D. Kuvshinov, N. Tyurina, A. Belinski, A. Krylov, P. Balanutsa, V. Chazov, A. Kuznetsov, P. Kortunov, A. Sankovich, A. Tlatov, A. Parkhomenko, V. Krushinsky, I. Zalozhny, A. Popov, T. Kopytova, K. Ivanov, S. Yazev, V. Yurkov, *Adv. Astron.*, 30L (2010)

V.M. Lipunov, E.S. Gorbovskoy, V.G. Kornilov, M.I. Panasyuk, A.M. Amelushkin, V.L. Petrov, I.V. Yashin, S.I. Svertilov, SHOK—the first Russian wide-field optical camera in space. *Space Sci. Rev.* (2017, this issue)

A.I. MacFadyen, S.E. Woosley, *Astrophys. J.* **524**, 262 (1999)

G. Milikh, J. Valdivia, K. Papadopoulos, Model of red sprite optical spectra. *Geophys. Res. Lett.* **24**(8), 833–836 (1997)

E. Nakar, *Phys. Rep.* **442**, 166 (2007)

A. Olinto, E. Parizot, M. Bertaina, G. Medina-Tanco, JEM-EUSO science, in *Proceedings of Science (ICRC2015)* (2015), p. 623

R. Orville, R. Henderson, Absolute spectral irradiance measurements of lightning from 375 to 880 nm. *J. Atmos. Sci.* **41**(21), 3180–3187 (1984)

A. Panaiteescu, W. Vestrand, *Mon. Not. R. Astron. Soc.* **387**, 497 (2008)

M.I. Panasyuk et al., *J. Cosmol.* **18** (2012). <http://lomonosov.simp.msu.ru/en/scientific-equipment-2/tus>

M.I. Panasyuk, M. Casolino, G.K. Garipov et al., The current status of orbital experiments for UHECR studies. *J. Phys. Conf. Ser.* **632**(1), 012097 (2015). doi:10.1088/1742-6596/632/1/012097

M.I. Panasyuk, S.I. Svertilov, V.V. Bogomolov et al., RELEC mission: relativistic electron precipitation and TLE study on-board small spacecrafet. *Adv. Space Res.* **57**(3), 835–849 (2016)

I.H. Park et al., *New J. Phys.* **15**, 023031 (2013). <http://uffo.skku.edu>

J. Paul et al., *C. R. Phys.* **12**, 298 (2011)

R. Perna et al., *Astrophys. J.* **585**, 775 (2003)

T. Piran, *Rev. Mod. Phys.* **76**, 1143 (2004)

A. Porcelli, Measurements of X_{\max} above 10^{17} eV with the fluorescence detector of the Pierre Auger Observatory, in *Proceedings of Science (ICRC2015)* (2015), p. 420

N. Produit et al., *Nucl. Instrum. Methods Phys. Res., Sect. A, Accel. Spectrom. Detect. Assoc. Equip.* **550**, 616 (2005)

G.D. Reeves, K.L. McAdams, R.H.W. Friedel, T.P. O’Brien, Acceleration and loss of relativistic electrons during geomagnetic storms. *Geophys. Res. Lett.* **30**(10), 1529 (2003). doi:10.1029/2002GL016513

G. Ricker et al., *Astrophys. J.* **571**, L127 (2002). <http://space.mit.edu/HETE/Welcome.html>

P.W.A. Roming et al., *Mem. Soc. Astron. Suppl.* **21**, 155 (2012)

V.A. Sadovnichii, V.V. Aleksandrov, T.B. Aleksandrova, E. Soto et al., Mathematical simulation of correction of output signals from the gravitoinertial mechanoreceptor of a vestibular apparatus. *Mosc. Univ. Mech. Bull.* **68**(5), 111–116 (2013)

V.A. Sadovnichiy, V.V. Alexandrov, T.B. Alexandrova, G.Yu. Sidorenko, N.E. Shulennina, E. Soto, Computer model of vestibular function in extreme conditions, in *Innovation Solutions for Space Mechanics, Physics, Astrophysics, Biology and Medicine*, ed. by V.A. Sadovnichiy, A.I. Grigoriev, M.I. Panasyuk (Moscow University Publishing House, Moscow, 2010), pp. 233–247 (in Russian)

V.A. Sadovnichiy, V.V. Alexandrov, S.S. Lemak, D.I. Bugrov, K.V. Tikhonova, R. Temoltz Avila, Robust stability, minimax stabilization and maximin testing in problems of semi-automatic control, in *Continuous and Distributed Systems II. Theory and Applications* (Springer, Berlin, 2015), pp. 247–265

V.A. Sadovnichiy, M.I. Panasyuk, S.Y. Bobrovnikov et al., First results of investigating the space environment onboard the Universitetskii-Tatyana satellite. *Cosm. Res.* **45**(4), 273–286 (2007). doi:10.1134/S0010952507040016

V.A. Sadovnichiy, M.I. Panasyuk, I.V. Yashin et al., Investigations of the space environment aboard the Universitetsky-Tat’yan and Universitetsky-Tat’yan-2 microsatellites. *Sol. Syst. Res.* **45**(1), 3–29 (2011). doi:10.1134/S0038094611010096

T. Sagawa, Telescope Array extension: TA \times 4, in *Proceedings of Science (ICRC2015)* (2015), p. 657

N. Sakaki, S. Ogio, F. Fenu et al., Expected acceptance of the KLNPVE/KEUSO space-based mission for the observation of ultra-high energy cosmic rays, in *Proceedings of Science (ICRC2015)* (2015), p. 647

R. Salvaterra et al., *Nature* **461**, 1258 (2009)

D. Semikoz, P. Tinyakov, M. Zotov, Detection prospects of the TA hotspot by space observatories (2016). [arXiv:1601.06363](https://arxiv.org/abs/1601.06363)

A. Shahmoradi, R. Nemiroff, *Mon. Not. R. Astron. Soc.* **411**, 1843 (2011)

Y.Y. Shprits, S.R. Elkington, N.P. Meredith, D.A. Subbotin, Review of modeling of losses and sources of relativistic electrons in the outer radiation belt I: radial transport. *J. Atmos. Sol. Terr. Phys.* **70**, 1679–1693 (2008a)

Y.Y. Shprits, D.A. Subbotin, N.P. Meredith, S.R. Elkington, Review of modeling of losses and sources of relativistic electrons in the outer radiation belt II: local acceleration and loss. *J. Atmos. Sol. Terr. Phys.* **70**, 1694–1713 (2008b)

H.C. Stenbaek-Nielsen, D.R. Moudry et al., Sprites and possible mesospheric effects. *Geophys. Res. Lett.* **27**(23), 3829–3832 (2000)

H. Su et al., Gigantic jets between a thundercloud and the ionosphere. *Nature* **423**(6943), 974–976 (2003)

S.I. Svertilov, M.I. Panasyuk, V.V. Bogomolov, A.M. Amelushkin, V.O. Barinova, V.I. Galkin, A.F. Iyudin, E.A. Kuznetsova, A.V. Prokhorov, V.L. Petrov, I.V. Yashin, Wide-field gamma-spectrometer BDRG: GRB monitor on-board the Lomonosov mission. *Space Sci. Rev.* (2017, this issue)

Y. Takahashi, *New J. Phys.* **11**, 065009 (2009). <http://jemeuso.riken.jp/en>

N.R. Tanvir et al., *Nature* **461**, 1254 (2009)

P. Tinyakov, M. Fukushima, D. Ikeda et al., TA anisotropy summary, in *Proceedings of Science (ICRC2015)* (2015), p. 326

H. Tokuno et al., *Nucl. Instrum. Methods Phys. Res., Sect. A, Accel. Spectrom. Detect. Assoc. Equip.* **676**, 54 (2012)

E.S. Tomilovskaya, I.B. Kozlovskaya, Effects of long-term space flights on the organization of the horizontal gaze fixation reaction. *Hum. Physiol.* **36**(6), 708–715 (2010)

N. Tyrina, V. Lipunov, V. Kornilov, E. Gorbovskoy, N. Shatskij, D. Kuvshinov, P. Balanutsa, V. Krushinsky, I. Zalozhnyh, A. Tlatov, A. Parkhomenko, K. Ivanov, S. Yazev, P. Kortunov, A. Sankovich, A. Kuznetsov, V. Yurkov, *Adv. Astron.*, 63T (2010)

M. Unger, Report of the working group on the composition of ultra-high energy cosmic rays, in *Proceedings of Science (ICRC2015)* (2015), p. 307

I. Valiño, The flux of ultra-high energy cosmic rays after ten years of operation of the Pierre Auger Observatory, in *Proceedings of Science (ICRC2015)* (2015), p. 271

N.N. Vedenkin, G.K. Garipov, P.A. Klimov et al., Atmospheric ultraviolet and red-infrared flashes from Universitetsky-Tatiana-2 satellite data. *J. Exp. Theor. Phys.* **113**(5), 781–790 (2011). doi:[10.1134/S1063776111130139](https://doi.org/10.1134/S1063776111130139)

W.T. Vestrand, P.R. Wozniak, J.A. Wren, E.E. Fenimore, T. Sakamoto, R.R. White, D. Casperton, H. Davis, S. Evans, M. Galassi, K.E. McGowan, J.A. Schier, J.W. Asa, S.D. Barthelmy, J.R. Cummings, N. Gehrels, D. Hullinger, H.A. Krimm, C.B. Markwardt, K. McLean, D. Palmer, A. Parsons, J. Tueller, A link between prompt optical and prompt big gamma-ray emission in big gamma-ray bursts. *Nature* **435**, 178 (2005)

E. Waxman, *Nucl. Phys. B, Proc. Suppl.* **151**, 46 (2006)

E.M. Wescott, D.D. Sentman, M.J. Heavner, D.L. Hampton, O.H. Vaughan Jr., Blue jets: their relationship to lightning and very large hailfall, and their physical mechanisms for their production. *J. Atmos. Sol.-Terr. Phys.* **60**, 713–724 (1998)

C. Winkler et al., *Astron. Astrophys.* **411**, L1 (2003). <http://www.isdc.unige.ch/integral>

G.T. Zatsepin, V.A. Kuz'min, Upper limit of the spectrum of cosmic rays. *JETP Lett.* **4**, 78 (1966)

B. Zhang et al., *Astrophys. J.* **703**, 1696 (2009)